Master Thesis

Laser stabilization to low-expansion Fabry-Pérot cavity

Quantum information group

Lund University, Sweden

Author:
Adam Wiman

Supervisor:
Lars Rippe

October 14, 2011

Abstract

During this thesis a frequency stabilization system for a dye laser system has been designed and partially built. The design is centered around a Fabry-Pérot cavity with a spherical spacer made of ultra low expansion glass. The system has been designed to stabilize the laser to a 2 Hz line width.

To be able to attain the desired performance the impact of different noise sources have to be considered. A number of support systems are needed to isolate the cavity from these noise sources. The main challenges lies in maintaining thermal stability of the cavity and isolating the cavity from mechanical vibrations. The low tolerance for noise also sets some limits on what electronics that can be used in the stabilization system. The ultimate performance limit is given by the thermal movements (Brownian motion) in the surface of the cavity mirrors.

The timeframe of the thesis set some limitations and the final alignment of the optics and performance measuerments of the system lies outside the scope of this project.

Populärvetenskaplig sammanfattning

En av laserns främsta egenskaper är att den sänder ut ljus som är enfärgat, alltså ljus som innehåller få färgnyanser. Detta examensarbete har fokuserat på att konstruera ett stabiliseringssystem för att ytterligare minska antalet nyanser.

I alla kontrollsystem krävs någon form av referens. Om du till exempel är ute och kör bil och vill köra med en hastighet av 90 km/h då måste du kunna mäta din hastighet på något sätt. Hur noga du måste kunna mäta hastigheten styrs av hur noga du vill veta att du kör i just 90 km/h.

För stabiliseringssystemet har en optisk kavitet använts som referens, en kavitet i detta sammanhanget innebär precis som det låter ett hålrum för ljuset. Hålrummet utgörs av två speglar riktade mot varandra. Precis som en hastighetsmätare mäter hur fort du kör används kaviteten för att mäta vilken färg ljuset har.

När ljus skickas in i den optiska kaviteten kommer en del av ljuset att gå rakt igenom kaviteten och en del ljus kommer att reflekteras, vad som händer beror på vilken färg ljuset har. Genom att utnyttja detta fenomen kan färgen på ljuset mätas. Vilka färger som kommer att gå rakt igenom kaviteten styrs av kavitetens längd, alltså avståndet mellan de två speglarna.

Målet har varit att konstruera ett system med en precision på 15 siffrors noggrannhet. Det motsvaras av att mäta avståndet till månen med en precision på en tusendels millimeter. Då avståndet mellan speglarna är det som avgör vilken färgnyans av ljuset som går rakt igenom kaviteten måste detta avstånd vara bestämt med 15 siffrors noggrannhet och inte ändras under den tid det tar att utföra ett experiment.

För att hålla spegelavståndet konstant krävs en rad åtgärder som isolerar kaviteten från omgivningen. Detta eftersom minsta lilla vibration, tryckförändring eller temperaturförändring påverkar avståndet mellan speglarna. Det är arbetet med att konstruera dessa system som tagit lejonparten av tiden under detta examensarbete.

Nomenclature

A/D Analog to digital

AOM Acousto-optic modulator

DDS Direct digital synthesizerr

EOM Electro-optic modulator

Eur Europium

FDT Fluctuation dissipation theorem

$FPGA$ Field programmable gate array

PDH Pound-Drever-Hall (scheme for locking to cavities)

PID Proportional–Integral–Derivative (commonly used type of controller)

Pr Praseodymium

SG Signal generator

UHV Ultra high vacuum

Y_2SiO_5 Yttrium silicate oxide

Contents

1 Introduction

Lasers have been around since 1960 when T.H. Maiman demonstrated the first laser [1]. Since then a lot of development has taken place and lasers have found their way into most peoples everyday life, for instance in the shape of DVD-players. A laser emits coherent light in a narrow frequency band, the width of the frequency band in which the laser is emitting is called the laser linewidth.

Very stable lasers have a narrow linewidth and a center frequency which drift very little over time. This kind of stable lasers are useful for a variety of different spectroscopy applications where a low noise figure is desired. At the moment the development of stable lasers are mainly driven by the needs from the research groups developing very precise clocks.

The most precise clocks today are using the frequency of some atomic transition in ions as a reference [2]. The problem is that these transition can't be probed continuously and therefore some kind of flywheel oscillator is needed that keep track of the time when measurements aren't done.

1.1 Clocks

Today the cesium clock is the global time standard. A transition between two hyperfine states in cesium 133 is used as reference, this transition lies a little below 9.2 GHz. This means that one second is defined as 9 192 631 770 periods of oscillation from this transition [3].

In a cesium clock a hydrogen maser is used as a flywheel oscillator, the maser have a very good short time stability and is therefore suitable for this task. The best cesium clocks today have an inaccuracy of 3×10^{-16} [4].

1.1.1 Optical clocks

By using a transition with a higher frequency the definition of a second can be made more precise. The second will then be defined as even more oscillations and the measurement can then be made more precise. The most precise clock in the world at the moment uses trapped aluminum ions where a transition at 1.121×10^{15} Hz (267 nm) is used as reference. This means

that the flywheel oscillator in this case has to be a laser instead of a maser because 1.121×10^{15} Hz is in the optical regime.

The most precise Al clocks at the moment have an inaccuracy of 8.6×10^{-18}, more than one order of magnitude better then the cesium clocks that are the current time standard [5]. To attain this low inaccuracy the laser that functions as flywheel oscillator needs to have a very high frequency stability.

1.2 Reason for constructing a stable laser

The reason an ultra-stable laser is designed and built during this thesis is not to use it for a clock application. The main research conducted in the group is focused on quantum computing in rare-earth-ion doped crystals. In recent years most of the experiments have been done using Praseodymium (Pr) doped Yttrium silicate oxide (YSO), Pr^{3+}:Y_2SiO_5. But to attain longer coherence times and thereby for instance extend the time information can be stored in a qubit other doping materials will have to be used. The next step is to use Europium (Eu) instead which when doped into YSO (Eu^{3+}:Y_2SiO_5) will have some optical transitions with a linewidth of only 122 Hz [6].To be able to probe such a narrow transition without introducing a lot of noise the laser used has to have a much narrower linewidth, in this case in the order of 10 Hz.

When the coherence time in the material is extended the time frame of a single experiment is also extended. This puts some additional performance requirements on the laser regarding frequency drift. When doing measurements on ions the phase error acceptable will be in the order of 5° and the longest experiments done will be 1 ms. This means that the laser has to have an absolute frequency stability in the order of 10 Hz. When the center frequency has drifted more than that the measurements have to be restarted.

1.3 Scope of the project

The scope of the thesis has been to research the necessary background information, design the complete system down to component level and order and mount the different components. Due to the time limitations of the master thesis the final optical alignment, construction of some electronics and testing of the system lies outside the scope of this thesis.

2 Laser stabilization

Many modern research lasers have some type of built in system for frequency stabilization. To improve the frequency stability of a laser beyond what the built in system is capable of an external cavity can be used as a reference. The error signal generated by the external reference can fed back to the control system in the laser to improve the frequency stability further.

2.1 Locking to a Fabry-Pérot cavity

Fabry-Pérot cavities are often used as the external reference. By studying the transmission spectrum for such a cavity, see figure 3.3, it is quite obvious that a fringe in the transmission spectrum can be used as a reference. Laser light is sent to the cavity and the light transmitted through the cavity is measured, by then tuning the laser frequency so the transmitted light is maximized all the time the laser frequency is locked to one of the transmission fringes.

Although this scheme might seem useful and simple it has some major drawbacks. If the intensity of the laser light varies it can't be distinguished from frequency variations, this means that a separate light intensity stabilization system is needed as well. An other problem is that the error signal is symmetrical, the same error signal is generated when the laser drifts up in frequency as when it drifts down in frequency. And lastly the response time of the control loop using the cavity is limited by the ringdown time of the cavity, see equation 3.3. The ringdown time or photon lifetime in a high finesse cavity can be in the order of μs which will impose some major limitations on the bandwidth of the system.

2.1.1 PDH Locking

To avoid the problems mentioned previously the Pound-Drever-Hall locking scheme can be used. Instead of using the transmitted light the reflected light is used, thereby the response time is not longer limited by the cavity ringdown time. Using the reflected light means that the intensity variations and frequency variations will be decoupled because the intensity should be kept at a minimum instead of at a maximum as when the transmitted light

is used [7]. The error signal will still be symmetrical, looking something like figure 2.1.

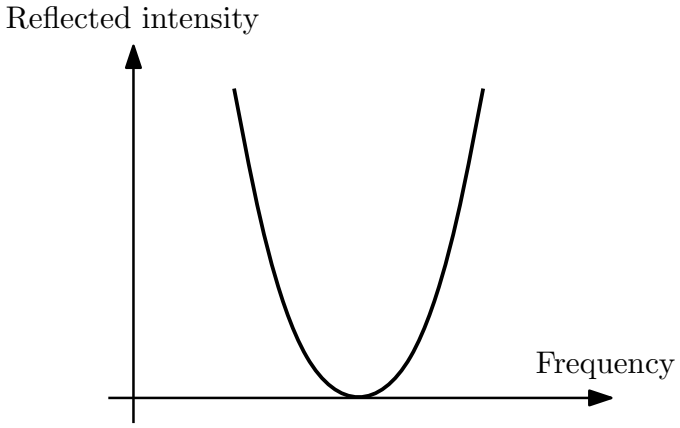

Figure 2.1: Reflected light intensity around a transmission fringe from a Fabry-Pérot cavity.

To get a sign sensitive detection of the frequency change a small phase modulation is created on the light with an EOM before the cavity. After the light have been modulated the electric field can be written as in equation 2.1.

$$E_{inc} = E_0 e^{i(\omega_0 t + \beta \sin \omega_m t)} \tag{2.1}$$

Where ω_0 is the frequency of the incident light, ω_m is the phase modulation frequency and β is the modulation depth. Equation 2.1 can be expanded using Bessel functions, if the modulation depth is small ($\beta < 1$) only three Bessel terms are needed to get a good approximation, see equation 2.2 [8].

$$\begin{aligned} E_{inc} &\approx E_0[J_0(\beta) + 2iJ_1(\beta)\sin(\omega_m t)]e^{i\omega_0 t} \\ &= E_0\left[J_0(\beta)e^{i\omega_0 t} + J_1(\beta)e^{i(\omega_0+\omega_m)t} - J_1(\beta)e^{i(\omega_0-\omega_m)t}\right] \end{aligned} \tag{2.2}$$

It's evident that the field consists of three frequency components, the main carrier and two sidebands. The side bands can be rewritten as in equation 2.3.

$$\begin{aligned} E_s &= E_0\left[J_1(\beta)e^{i(\omega_0+\omega_m)t} - J_1(\beta)e^{i(\omega_0-\omega_m)t}\right] \\ &= E_0 J_1(\beta)e^{i\omega_0 t} 2i\frac{e^{i\omega_m t} - e^{-i\omega_m t}}{2i} \\ &= E_0 J_1(\beta)e^{i\omega_0 t} 2i\sin(\omega_m t) \\ &= 2E_0 J_1(\beta)e^{i\omega_0 t + \frac{\pi}{2}}\sin(\omega_m t) \end{aligned} \tag{2.3}$$

The sidebands will always be out off resonance with the cavity and therefore always reflected. The main carrier on the other hand will only be reflected when it's off resonance with cavity. Depending on how far off resonance the main carrier is the phase of the detected signal will vary. To

measure the phase of the detected signal it's mixed with the signal driving the EOM. By low pass filtering the mixed signal an error signal can be attained.

A basic setup for PDH-locking can be seen in figure 2.2. To separate the light incident on the cavity from the light reflected a $\lambda/4$ - plate and a polarizing beam splitter is used. The light reflected from the cavity will pass through the $\lambda/4$ - plate two times and have its polarization direction rotated a total of 90^o. This make it possible to pick of the reflected light with a polarizing beam splitter.

The phase measurement of the detected signal is done with a mixer and a low pass filter. A phase shifter is also used to compensate for different signal path lengths.

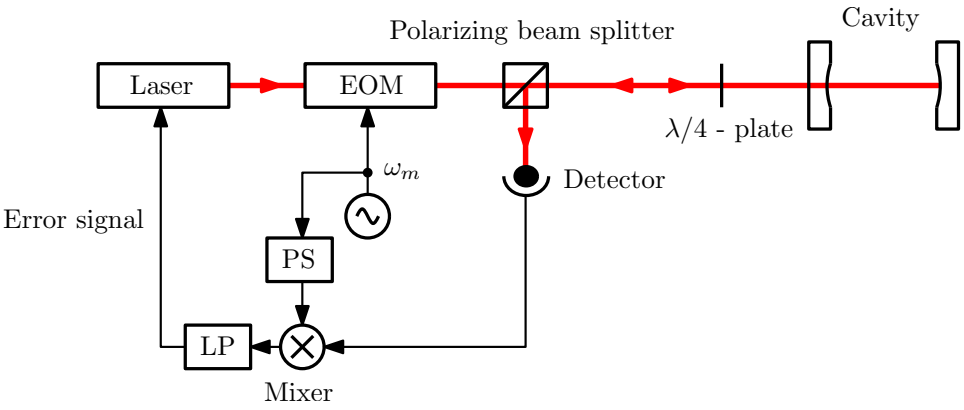

Figure 2.2: Setup for PDH locking.

The performance of PDH locking is fundamentally limited by shot noise. Shot noise is noise due to the quantified nature of light. In applications where a Fabry-Pérot cavity is used noise caused by the cavity sets the performance limit and not the shot noise from PDH locking.

2.2 Fiber noise cancellation

Optical fibers are commonly used to couple light from one position to an other, it can be over many kilometers or only a few meters inside a lab. A fiber is never completely still, there will be movements due to thermal fluctuations and there will be mechanical vibrations from the environment coupling to the fiber. These length changes and vibrations will couple to the light passing through the fiber. In most applications these effects can be neglected because they are so small. But in applications where very frequency stable light is sent through the fiber these variations will ruin the stability of the laser light and therefore have to eliminated.

The basic working principle of a fiber noise cancellation system is that some light is sent through the fiber and then compared with light that hasn't passed through the fiber. The phase noise caused by the fiber can thereby be measured and compensated for. A basic setup for fiber noise cancellation

can be seen in figure 2.3. The light incident to the fiber has some frequency f_l, the frequency stability of that light should be maintained.

The light passes through an AOM and the light diffracted will be shifted in frequency $f_{osc} + f_{reg}$. The diffracted light is sent through the fiber. After passing the fiber some of the light is picked of and sent back through the fiber. The light returning will pass through the AOM again and will be frequency shifted once more with $f_{osc} + f_{reg}$. The returning light will then be picked of by an optical isolator and sent to a photo diode.

Part of the light incident to the system will not by diffracted by the AOM, it will pass through the AOM unaffected and is then reflected back through the AOM again. It will then also be picked of by the optical isolator and sent to the photo diode.

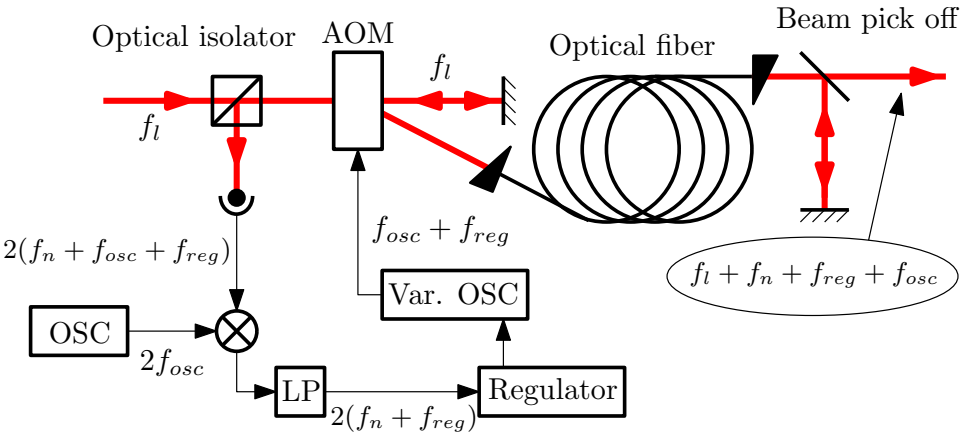

Figure 2.3: Fiber noise cancelation scheme.

The two overlapping beams on the photo diode will create a beating and the difference in frequency will be measured, $2(f_m + f_{osc} + f_{reg})$. This signal is mixed with two times the driving frequency for the AOM and low pass filtered to get rid of the $2f_{osc}$ frequency. The remaining signal, $2(f_n + f_{reg})$, is sent to a regulator as an error signal to be minimized. The oscillator driving the AOM has to be variable and the control signal from the regulator is used to control the frequency modulation of the oscillator.

The laser light passing through the fiber will have the frequency $f_l + f_n + f_{reg} + f_{osc}$ which means that if the regulation works and $f_n = -f_{reg}$ the light will be unaffected by the noise introduced by the fiber. The light will be shifted with the frequency f_{osc} but the stability will be maintained if the oscillator frequency is at least as stable as the light passing through the fiber [9].

2.3 Allan variance

To compare the frequency stability of different clocks/lasers a measure is needed that is applicable to different types of clocks. The measure should give an objective measure independent of which type of noise that is domi-

nant for a specific clock type. Standard variance is one option, see equation 2.4, where f_i are frequency measurements and N is the number of samples.

$$\sigma_N^2 = \frac{1}{N-1} \sum_{i=N}^{N} \left(f_i - \frac{1}{N} \sum_{i=1}^{N} f_i \right)^2 \tag{2.4}$$

It turns out that standard variance is divergent for some types of noise commonly present in clocks, [10] page 13. This means that standard variance varies with the number of samples N and is therefore unsuitable.

The M-sample variance, also called Allan variance, provides a way to compare the frequency stability of different clocks. The Allan variance is given by equation 2.5, where τ is the sample period and $\bar{f}_i$ is the frequency values averaged over the sampling interval τ, [10] page 14.

$$\sigma_f^2(\tau) = \frac{1}{2(M-1)} \sum_{i=1}^{M-1} \left(\bar{f}_{i+1} - \bar{f}_i \right)^2 \tag{2.5}$$

It has been shown that any Allan variance with a finite number of measurements M can be recalculated to a two sample variance [11]. Therefore only the two sample variance is used with M=2. When the Allan deviation is calculated either overlapping samples or non-overlapping samples can be used, se figure 2.4. Care must be taken when overlapping samples are used because the different samples are then not completely uncorrelated. The benefit with using overlapping samples is that the confidence interval is improved without needing to increase the number of samples.

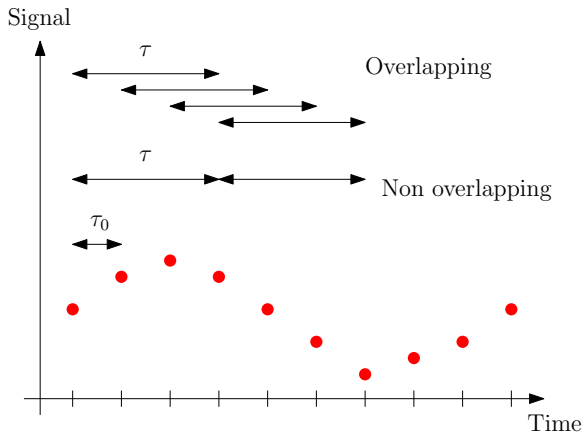

Figure 2.4: Different types of sampling that can be used for calculating the Allan variance.

The Allan variance for non-overlapping samples is given by equation 2.5 and the Allan variance for overlapping samples is given by equation 2.6. Where $\tau = m \cdot \tau_0$ is the sample period, m is averaging period and $\bar{f}_i$ is the frequency values averaged over the sampling interval τ, [10].

$$\sigma_f^2(\tau) = \frac{1}{2m^2(M-2m+1)} \sum_{j=1}^{M-2m+1} \sum_{i=j}^{j+m-1} \left(\bar{f}_{i+m} - \bar{f}_i\right)^2 \tag{2.6}$$

3 Equipment

The stabilization system consists of almost a hundred different components. In this chapter a brief introduction will be given to the most important types of components used.

3.1 Optics

3.1.1 Acousto optical modulator

An acousto optical modulator, AOM, is a device that utilizes the acousto optical effect to manipulate light. In certain materials acoustic waves can be used to manipulate the refractive index of the material and thereby also the light passing through the material.

A schematic sketch of an AOM can be seen in figure 3.1 with the key components illustrated. The light passes through a piece of glass or crystal, the sound waves are created by a transducer and will also propagate through the crystal. An absorber or a slanted edge is often used to prevent reflected sound waves to interact with the light.

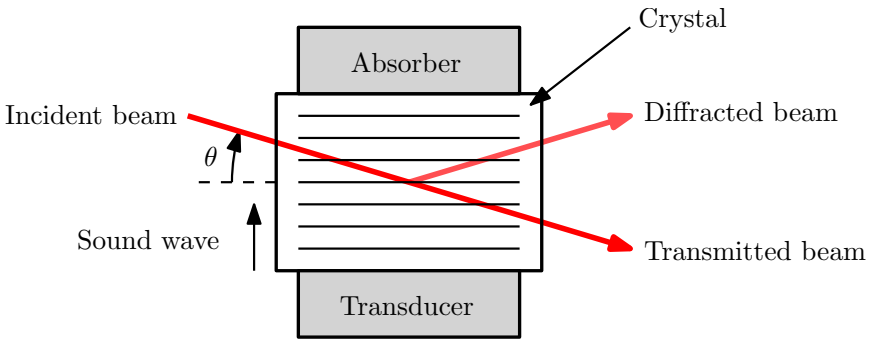

Figure 3.1: Operating principle of an AOM, the angle θ is called Bragg angle.

Maximum diffraction of light will take place when the angle between the incident light and and sound waves fulfill the Bragg condition, see equation 3.1, [12] page 806.

$$sin(\theta) = \frac{\lambda f_s}{2v_s} \tag{3.1}$$

Where θ is the Bragg angle (see definition in figure 3.1), f_s is the sound frequency, v_s is the sound velocity inside the AOM crystal and λ is the light wavelength. The response time off an AOM is limited by the speed of sound inside the crystal. When a change of sound frequency is made the sound has to propagate from the transducer to the volume of the crystal where the light passes through the crystal before any changes of the light modulation takes place.

3.1.2 Electro optical modulator, EOM

Some materials change their refractive index when subject to a constant or low frequency electric field. This phenomena can be used to modulate light by constructing a device where the light passes through the material while a voltage is applied over the material, [12] page 835. In figure 3.2 the key components in an EOM are illustrated.

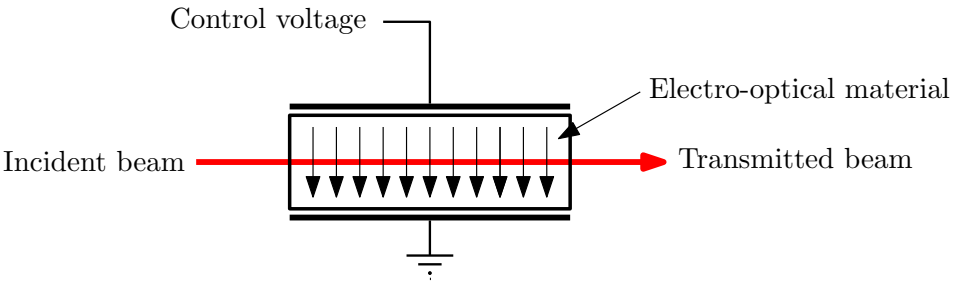

Figure 3.2: Operating principle of an EOM.

3.1.3 Fabry-Pérot cavity

Basic concepts

A Fabry-Pérot cavity consists of two mirrors facing each other making up the cavity. The transmission spectrum of the cavity is primarily affected by the reflectivity of the mirrors and the spacing between them. Two typical transmission spectrums can be seen in figure 3.3.

A Fabry-Pérot cavity is usually characterized by it's finesse, $\mathscr{F}$. Two other useful measures to consider when working with Fabry-Pérot cavities are the half maximum full width of the transmission fringes, $\delta\lambda$, and the transmission fringe spacing $\Delta\lambda$. See equation 3.2 where R is the reflection of the mirrors used and L is the spacing between the mirrors, [13] page 423 and [14] page 433.

$$\mathscr{F} = \frac{\pi\sqrt{R}}{1-R} \qquad \delta\lambda = \frac{\Delta\lambda}{\mathscr{F}} \qquad \Delta\lambda = \frac{c}{2L} \tag{3.2}$$

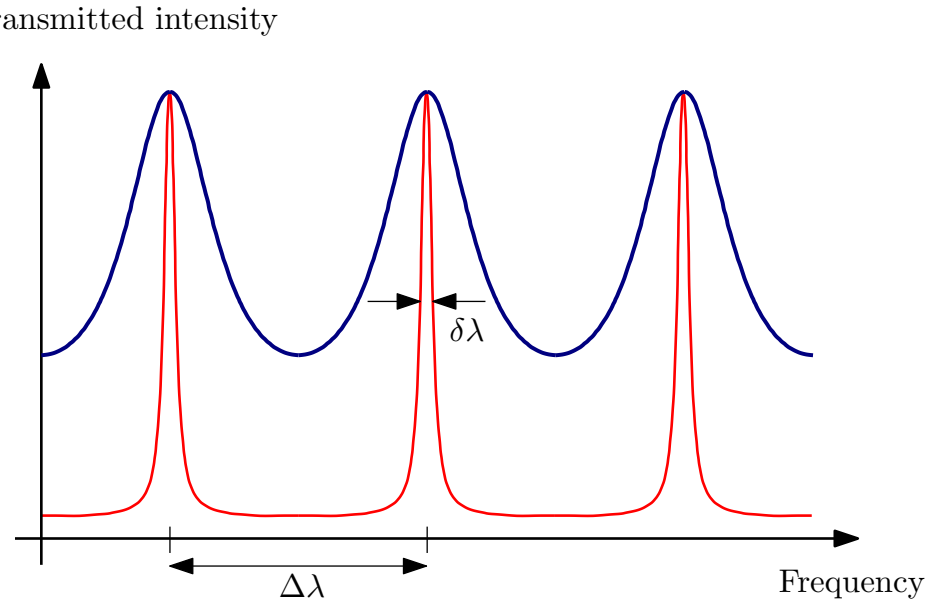

Figure 3.3: Transmission spectrums from two Fabry-Pérot cavity with different finesse but with the same mirror spacing.

The cavity ringdown time for a cavity is a measure for how quickly the cavity responds to changes in the light intensity incident on the cavity. It basicly measures how long it takes for the intensity to build up inside the cavity when the light is turned on or vice versa decay when the light is turned off. The ringdown time is defined as in equation 3.3, [15].

$$\tau = \frac{1}{2\pi\delta\lambda} \tag{3.3}$$

Stable high finesse cavities

When designing Fabry-Pérot cavities for frequency stabilization systems there are two major things to consider to achieve high stability. Firstly the mirrors should have very high reflectivity or be spaced far apart to attain sharp and well defined transmission fringes. This will govern how exact the stabilization can be made. Secondly the distance between the mirrors should be kept as constant as possible. If the distance changes the transmission fringes will shift in frequency. The laser will be locked to one of the fringes and it will therefore also shift in frequency when the fringe shift.

Manufacturing high reflectivity mirrors is a demanding process and only a few companies in the world are able to produce mirrors with the needed reflectivity (R=>99.999%) for high finesse cavities. It's also tricky to design a cavity that is able to keep the distance between the mirrors constant. This is a question of designing the cavity geometry and choosing the right materials for the different parts of the cavity.

Fabry-Pérot cavities used for frequency stabilization applications usually consists of three parts, two mirrors and a spacer upon which the mirrors are

attached, see figure 3.4. The mirrors are attached to the spacer with optical contact bounding. It's a process where two surfaces are polished completely flat and then put into contact with each other, if they are polished flat enough they will attach to each other. The benefit of using optical contacting is that no adhesive is needed which otherwise could ruin the thermal and mechanical properties of the cavity.

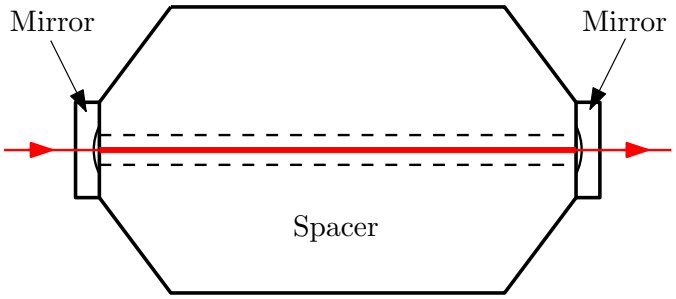

Figure 3.4: Sketch of a Fabry-Pérot cavity.

Thermal movements in the cavity mirrors

The fundamental stability limit for systems using Fabry-Pérot cavities are given by the thermal noise (Brownian motion) due to atom movements in the mirror surfaces. The amount of random movement in a material is related to the mechanical loss in the material by the fluctuation dissipation theorem, FDT, [16]. Numerical simulations suggest that mirrors substrates made of fused silica is the best choice to minimize the noise due to thermal movements in the mirrors, [17].

Thermal expansion

To minimize the effect of thermal variations of the cavity the spacer has to made of some material with a very low thermal expansion coefficient. The material used most frequently in recent years is a ultra low expansion glass, ULE, from *Corning* [18, 19, 20]. ULE is a titania doped silica glass that has a very low thermal expansion, to first order it doesn't expand at all, but it exhibits some changes to second order [21]. To minimize the effect from the changes the cavity is usually kept at the second order minimum expansion temperature.

When a cavity is kept at its minimum expansion temperature it still exhibits some sensitvity to thermal fluctuations. This is partly due to expansions of the spacer but a factor contributing to the sensitivity with the same order of magnitude is the thermal expansion of the dielectric coatings on the cavity mirrors [19]. This is quite surprising because the thickness of these coating are in the order of a few μm and the a spacer is almost one dm long.

A problem arises when the mirror substrates are made of fused silica and the spacer is made of ULE. The two materials have different temperature

expansion coefficients which means that temperature changes will lead to larger size changes in fused silica than in ULE. The two materials are rigidly attached to each so temperature fluctuations will lead to deformations of the mirror substrates. To minimize the effect of this a ring of ULE can be attached to the backside of the fused silica mirror, see figure 3.5, [22].

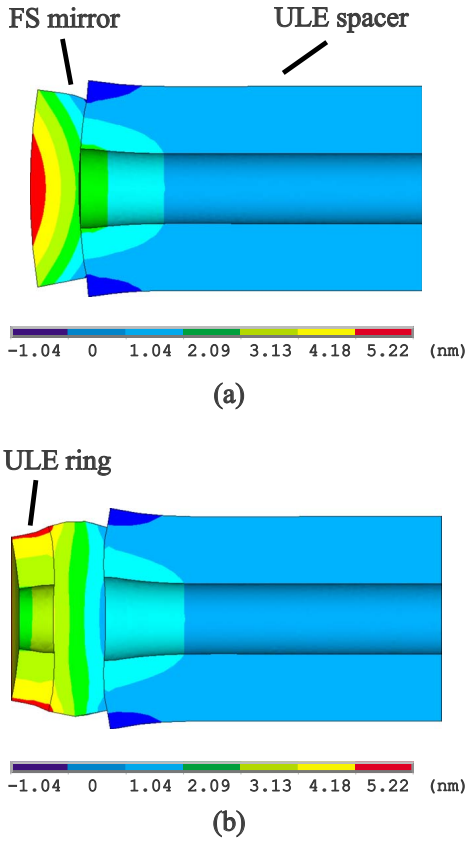

Figure 3.5: FEM simulation of deformation after 1 K temperature change. (a) shows a ULE spacer with a mirror made of fused silica optically contacted to it. (b) shows the spacer and the mirror with a compensation ring made of ULE contacted to the mirror. Figure taken from [22].

Mechanical vibrations

Mechanical vibrations of the cavity will couple directly to the light inside the cavity and thereby ruin the stability. The major concern is vibrations in the direction of the cavity's optical axis. To minimize the sensitivity to vibrations cavities have been mounted vertically with a mount at the midplane of the cavity, see figure 3.6. If the cavity experience a force directed upward the top part will be compress and the bottom part will be extended. If the cavity has the same length above as below the mount the length of the cavity won't change to first order, [23].

The drawback with vertically mounted cavities is that they are only kept

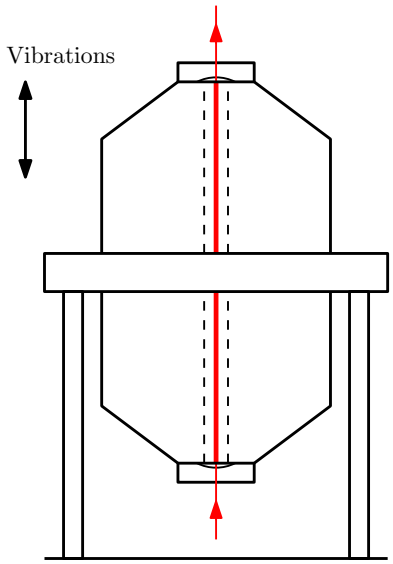

Figure 3.6: Vertically mounted cavity.

in place by gravity which makes the system quite fragile and sensitive to forces bigger than one g. An alternative is to have a spherical spacer instead, it will also be symmetrical and therefore not so sensitive to vibrations. To maintain the symmetry it should be mounted in two points, the question is which angle it should be between the mounting axis and the optical axis. If the mounting angle is perpendicular to the optical axis any increase in the force applied at the mounting points will transform to an elongation of the cavity length. If the mounting axis and the optical axis are parallel any increase in the force applied by the mount will transform to a compression of the cavity, see figure 3.7. It turns out that there is a "squeeze insensitive" angle at 52.69° between the optical axis and the mounting axis where the cavity length is insensitive to changes in the force applied by the mount to first order [20].

3.2 Electronics

3.2.1 Peltier element

A peltier element is a device that utilize the Peltier-Seebeck effect to either convert a temperature difference into an electrical current or vice versa convert an electrical current into a temperature difference. By varying the control current size and polarity the heat transfer direction and amount can be controlled.

A peltier element consists of varying p-doped and n-doped thermoelements connected in series electrically and in parallel thermally, see figure 3.8. When a electrical current is driven through the thermoelements holes will carry the current in the the p-doped material and electrons will carry the current in the n-doped material. The thermoelements should be man-

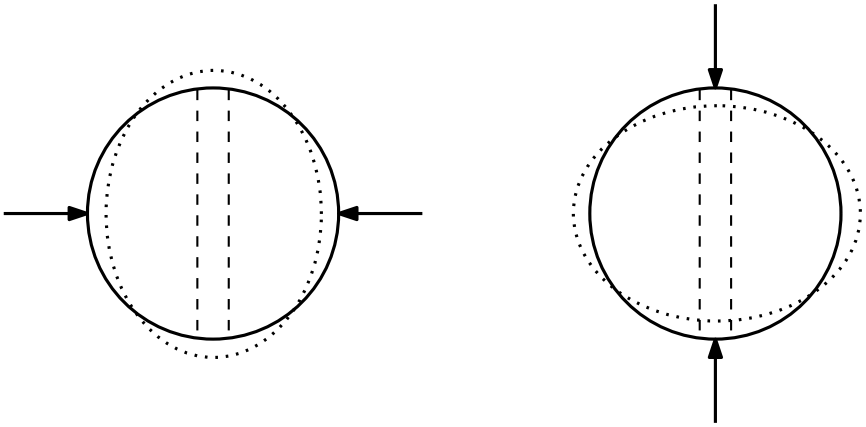

Figure 3.7: Deformation of a spherically shaped cavity spacer, the dashed lines indicate the direction of the optical axis.

ufactured of materials with a low thermal conductivity and with a high thermoelectrical effect. This means materials where a electrical potential difference give rise to a temperature difference, [24] page 164. See figure 3.8 for a illustration of a peltier element.

The peltier elements are sensitive to external forces and care has to be taken when they are handled. Pressure should be applied to achieve good thermal contact between the surface the peltier element is attached to and the peltier element. Peltier elements can't be cleaned in an ultrasonic bath and it should not be run without being connected to a heat sink [25].

3.3 Vacuum equipment

3.3.1 CF flange standard

CF flanges are commonly used in ultra high vacuum applications and are specified to operate down to $< 1.3 \times 10^{-13}$ mbar in the temperature range -196°C to 450°C. The flanges are unisex and are equipped with a knife edge. To seal a connection a gasket, usually made out of copper, is put between the flanges. When the flanges are bolted together the knife edges cuts into the softer gasket material and thereby seals the system. The copper gaskets are one time use only, [26].

When assembling the connections the right torque has to applied to the bolts, see table 3.1. It's also important that the bolts are tightened in a star pattern to assure that an even pressure is applied over the gasket.

Table 3.1: Tightening torque required for bolts when connecting CF flanges, [27].

Dimension	**Flange OD**	**Bolts used**	**Bolt torque**
DN40CF	70 mm	6 × M6	16 Nm
DN150CF	203 mm	20 × M8	20 Nm

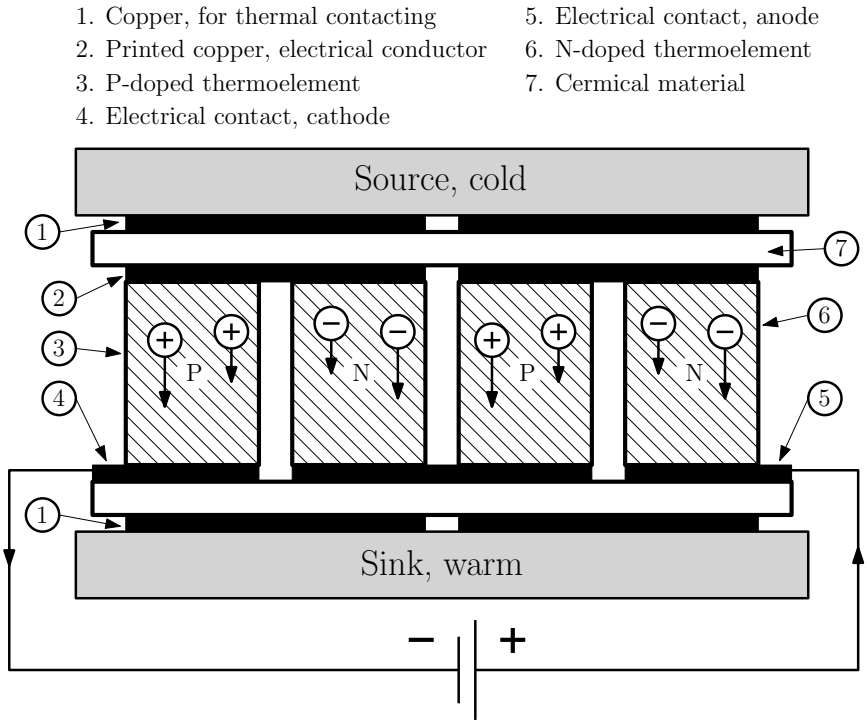

Figure 3.8: Cross section of a peltier element.

3.3.2 Diaphragm pump

Diaphragm pumps are mechanical pumps used for low vacuum applications. The key components in diaphragm pumps can be seen in figure 3.9. A crankshaft drives the a rod (4) connected to a diaphragm (3), when the diaphragm is moved back and forth the size of the suction chamber (8) changes and the gas in the chamber is compressed. To achieve a pumping effect two valves (6) are used to control the flow of the gas. The ultimate pressure of a diaphragm pump is limited by the pressure difference needed to open the valve into the suction chamber. This usually limits the ultimate pressure attainable with a single stage diaphragm pump to around 70 mbar, [28] page 62.

3.3.3 Turbomolecular pump

Turbomolecular pumps have a design somewhat similar to turbines and jet engines with rotors and stators. The basic outline of a turbomolecular pump can be seen in figure 3.10. The rotors (2) are angeled blades that rotates with high velocity. They set the gas molecules into motion and due to the angle of the blades the gas molecules will have a velocity distribution directed downwards into the pump. Every rotor is paired with a stator, the stator functions as baffle and hinders molecules from later compression stages flow backwards in the pump.

The angle of the blades are steeper at the inlet of the pump to allow for

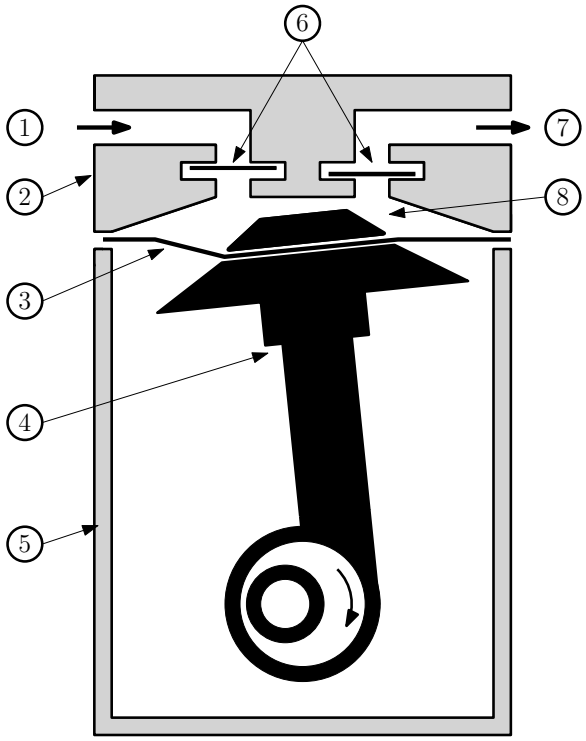

1. Inlet
2. Head cover
3. Diaphragm
4. Connecting rod
5. Housing
6. Valves
7. Outlet
8. Suction chamber

Figure 3.9: Operating principle of a diaphragm pump.

high gaseous flow. Near the outlet of the pump, where the pressure difference is smaller, the blades are mounted at a flatter angle to prevent backflow. A turbo molecular pump is usually not able to compress gas to atmospheric pressure and therefore need a backing pump to work efficiently,[28] page 81.

Some turbomolecular pumps are able to reach an ultimate pressure of 10^{-12} mbar but it varies a lot between different models.

3.3.4 Ion Getter pump

Ion getter pumps are used in vacuum systems where ultra high vacuum is needed. The key components of an ion pump can be seen in figure 3.11. A permanent magnet (3) encloses the whole pump body to create a strong magnetic field. To achive pumping effect a high voltage is applied between the Penning cells (5) and the titanium pumping elements (4,6), the high voltage will accelerate electron from the anode (5) to the cathodes (4,6). Due to the high magnetic field the electrons will follow helical trajectories when moving toward the cathodes, this will significantly extend the path the electrons have to travel to reach the cathode and thereby increase the density of free electrons moving inside the penning cells.

Gas molecules entering the ion pump and the penning cells have a high probability of getting hit by an electron, when this happens the gas molecule will be ionized. The ionized molecule will be accelerated towards the pumping elements (4,6) by the electric field. The effect of the magnetic field is

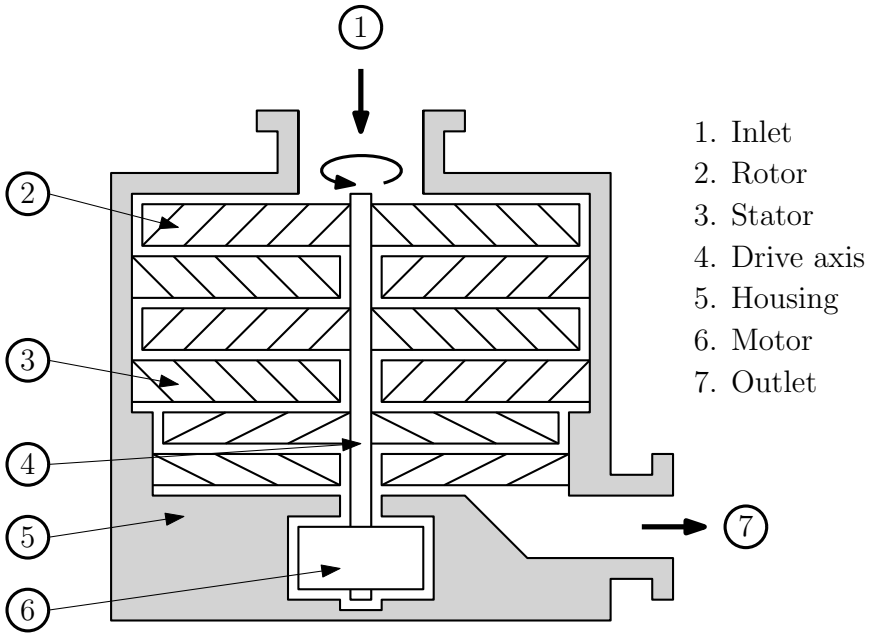

Figure 3.10: Operating principle of a turbomolecular pump.

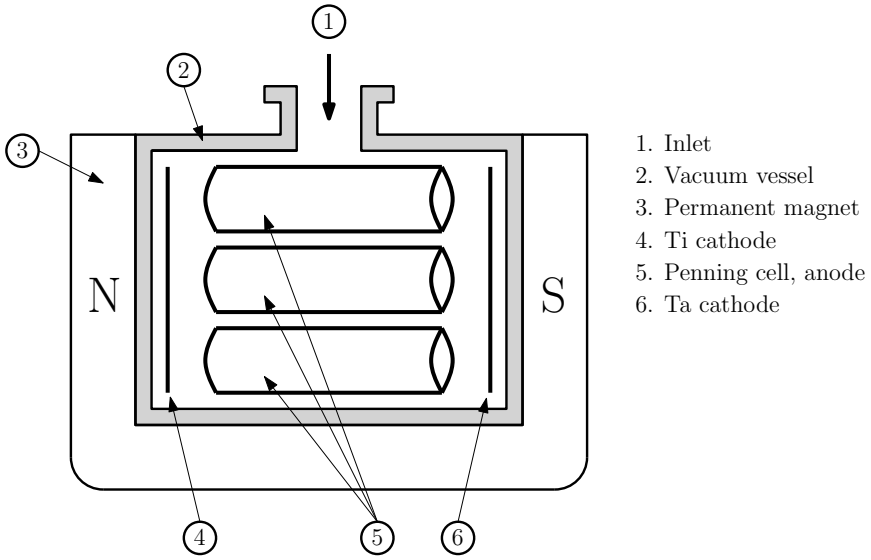

Figure 3.11: Operating principle of an ion pump.

much smaller on the ions than on the electrons due to the ions considerably higher mass. When the ions hit the pumping elements they are captured, the capturing process differs depending on which type of ion it is.

Most ions, other than noble gases, will react chemically with the titanium pumping element by a sputtering process. When the ion hits the titanium element it will sputter titanium away from the surface, this titanium will form an reactive surface on neighboring parts inside the pump, these surfaces will then chemically bind gas molecules that come into contact with them.

In addition to the sputtering process gas is also pumped by the sorption effect. This process is important for pumping noble gases but apply to all types of ions. When the ions impact the pumping elements with high enough energy they can penetrate deeply into the material, in the order of 10 atomic layers deep. This pumping effect is not permanent because the cathode slowly erode away due to the sputtering process.

Noble gases that impact the pumping elements with low velocities steal one electron from the surface and are then deflected. These molecules are permanently pumped when they impact some other part of the pump then the pumping elements with a high velocity, they will the be permanently buried because no other part then the cathodes are eroded. To increase this effect one titanium pumping element can be replaced with a tantalum element, noble gas ions incident on the tantalum element have much higher probability of being reflected and therefore increase the permanent pumping of noble gases, [29].

An ion getter pump can start pumping at as high pressures as 1×10^{-4} mbar but it will drastically shorten the lifetime of the pumping elements to about one procent compared to pumping at 1×10^{-6} mbar. Ion pumps generally are able to create a ultimate pressure in the range of 1×10^{-10} to 1×10^{-11}.

4
System design

Laser systems similar to the system designed during this master thesis have been demonstrated numerous times, [30, 31, 18, 20]. The design of the system in this thesis mostly resembles the system described in [19]. Before the design work started a visit was made to Münich and the Max Planck institute to learn more about the stabilization systems they have built.

The stabilization system constructed during this thesis is a replacement for an existing system, this meant that the laser system together with some other components were already in place when the work began. To give the reader a comprehensive picture the whole system is described in the following chapter. The format Bxx00 will be used to name all major components as it has been used in previous texts regarding this laser system, please see [32] for details on work previously done on the system.

4.1 System overview

The laser system can be broken down into a number of subsystems. The dye laser with it's solid state pump laser is used to generate the light. To lock the frequency of the laser light to the optical length of the cavity, which is used as the reference, a frequency stabilization system is needed. The rest of the subsystems are built to suppress different noise sources that would otherwise compromise the frequency stability of the laser. The supports systems needed for noise suppression are a frequency shifting system for the laser light, a fiber noise cancellation system, a laser intensity stabilization system, a camera system to facilitate the alignment of the optical components, a temperature stabilization system for the cavity, a vibration isolation system for the cavity and a vacuum system.

A drawing of the complete optical setup can be seen in figure 4.1 and an overview of all major electronic components can be seen in figure 4.2. A complete listing of all components on the optical table can be found in table 4.1 and a complete listing of all electronic components can be found in table 4.2.

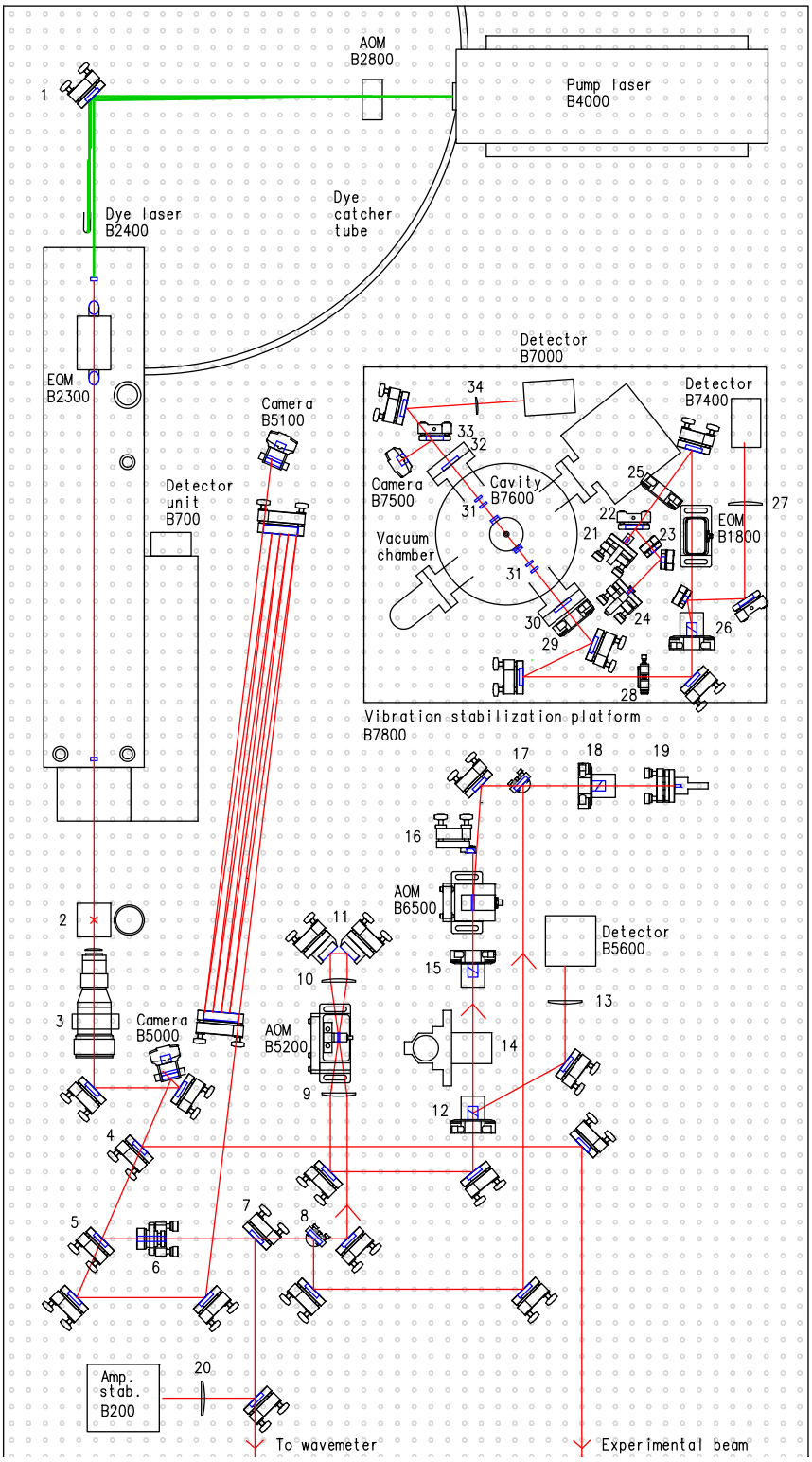

Figure 4.1: Overview of the optical components.

Table 4.1: Listning of all major components in figure 4.1. For explanations of components named Bxx00 please see table 4.2.

Nbr	Component type	Manufacturer	Model
1	High power mirror	CVI	-
2	Periscope, from 135 mm to 75.4 mm	Thorlabs	P200/M, C1501/M
3	Zoom beam expander	Sill Optics	S6ASS2075/067
4	Beam pick-off	Thorlabs	BST10
5	Mirror with polished back surface	CVI	BBD1-PM-1037-C
6	Beam expander, 2x	Thorlabs	BE02M-A
7	Beam pick-off	Thorlabs	BSF10-A1
8	Flip mirror	New Port	9891-M
9	Positive lens	Thorlabs	LA1145-A
10	Positive lens	Thorlabs	LA1145-A
11	Rectangular mirrors	Altechna	-
12	Polarizing beam splitter	Foctek	GPB7008
13	Positive lens	Thorlabs	LA1608-A
14	Faraday rotator	Leysop	FOI 5/57
15	Polarizer	Foctek	GLH8008
16	D-shaped mirror	Thorlabs	BBD1-E02
17	Flip mirror	New Port	9891-M
18	Polarizer	Foctek	GLH8008
19	Beam coupler	Schäfter Kirchhoff	60SMS-1-4-M5-33
20	Positive lens	-	-
21	Beam collimator	Schäfter Kirchhoff	60FC-4-M5-33
22	Plate beam splitter	Thorlabs	BST10
23	Line filter	Thorlabs	FL05635-10
24	Diode laser, 635 nm	Thorlabs	CPS180
25	Polarizer	Casix	PGL8308
26	Polarizing beam splitter	Foctek	GPB7008
27	Positive lens	Thorlabs	LA1608-A
28	Positive lens	CVI	LPX-13.0-22.3-C
29	$\lambda/4$-plate	Thorlabs	AQWP05M-630
30	Vacuum viewport	TSL	-
31	Isolating window	Thorlabs	WG10530-A
32	Vacuum viewport	TSL	-
33	Plate beamsplitter	Thorlabs	BSW10
34	Positive lens	Thorlabs	LA1608-A

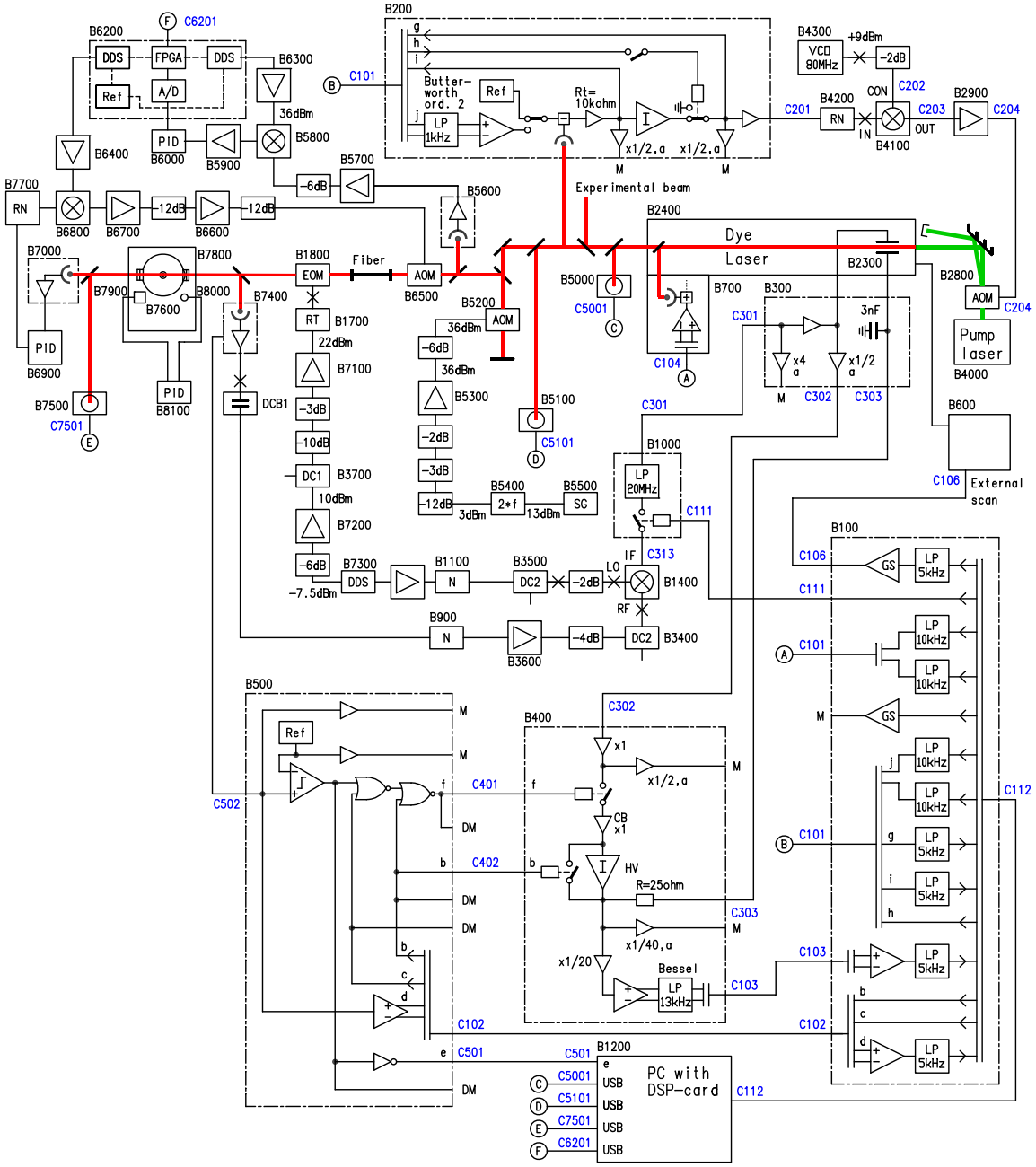

Figure 4.2: Overview of the electronic system, please see table 4.2 for a complete listing of all components.

Table 4.2: Listning of all major components in figure 4.2. Information regarding components B100 - B4300 can be found in [32].

Nbr	**Component type**	**Manufacturer**	**Model**
B100	Break-out box	-	-
B200	Amplitude stabilization	-	-
B300	EOM low-voltage generator	-	-
B400	EOM high-voltage generator	-	-
B500	Suspend regulation controller	-	-
B600	Dye laser, external scan	Coherent	699-21
B700	Dye laser, detector unit	Coherent	699-21
B900	Diplexer notch filter	-	-
B1000	Low-pass and notch diplexer	-	-
B1100	Notch diplexer filter	-	-
B1200	Laser control PC	-	-
B1400	Phase-detector	Mini-Circuits	RPD-2
B1700	Resonance tank for EOM	-	-
B1800	50 MHz EOM	New Focus	4002-M
B2300	Intracavity EOM	Linos PM25	50 2075
B2400	Dye laser	Coherent	699-21
B2800	Amplitude stabilization AOM	Brimrose	FQM-80-1
B2900	5W amplifier	Mini-Circuits	ZHL-5W-1
B3400	Directional coupler	Mini-Circuits	ZX30-20-4
B3500	Directional coupler	Mini-Circuits	ZX30-20-4
B3600	Amplifier	Mini-Circuits	ZFL-500HLN
B3700	Directional coupler	Mini-Circuits	ZMDC-20-3
B4000	Pump laser	Coherent	Verdi V6
B4100	Mixer	Mini-Circuits	ZAD-3
B4200	Impedance converter	-	-
B4300	80MHz VCO	Mini-Circuits	ZOS-100
B5000	Realignment camera	Thorlabs	DCC1545
B5100	Realignment camera	Thorlabs	DCC1545
B5200	Frequency shifter AOM	Brimrose	GPF-1125-750-590
B5300	Amplifier	Mini-Circuits	ZHL-30W-252
B5400	Frequency doubler	Mini-Circuits	FK-3000+
B5500	Signal generator	Rohde & Schwarz	SML01
B5600	Photo diode	Hamamatsu	S9055
B5700	Amplifier	Mini-Circuits	ZX60-3018-S+
B5800	Phase detector	Mini-Circuits	SYPD-2
B5900	Low frequency amplifier	See appendix B for schematics.	- -
B6100	PID Regulator	New Focus	LB1005
B6200	Frequency generation	-	-
B6300	Amplifier	Mini-Circuits	ZX60-3018-S+

Table 4.2: Listning of all major components in figure 4.2. Information regarding components B100 - B4300 can be found in [32].

Nbr	**Component type**	**Manufacturer**	**Model**
B6400	Amplifier	Mini-Circuits	ZX60-3018-S+
B6500	Fiber noise cancel. AOM	Isomet	1250C
B6600	Amplifier	Mini-Circuits	ZHL-1-2W-S
B6700	Amplifier	Mini-Circuits	ZX60-3018-S+
B6800	Variable attenuator	Mini-Circuits	ZMAS-3
B6900	PID Regulator	SRS inst.	SIM960
B7000	Photo diode	Hamamatsu	S5971
B7100	Amplifier	Mini-Circuits	ZHL32A
B7200	Amplifier	Mini-Circuits	ZX60-43-S+
B7300	DDS	Analog devices	AD9959
B7400	Photo diode	Hamamatsu	S9055
B7500	Realignment camera	Thorlabs	DCC1545
B7600	Fabry-Pérot cavity	Advanced Thin films	-
B7700	Voltage to current converter	See appendix B for schematics.	-
B7800	Vibration isolation platform	HWL	TS140
B7900	Peltier element	Custom Thermoelectrics	01701-9L31-09B
B8000	Thermistor	EPOTEK	871-B57560G203F
B8100	Temperature controller	Thorlabs	TED200

4.2 Dye laser system

The dye laser used is a slightly modified Coherent 699-21 (B2400) pumped with a Coherent Verdi V6 $Nd{:}YVO_4$ solid state diode laser (B4000). In the dye jet laser the lasing takes place in a free flowing jet stream, fluctuations in the jet thickness causes quite large frequency shifts in the output light. Frequency errors in the range 10 Hz to 1 kHz are compensated by moving one of the cavity mirrors which is mounted on a piezoelectric actuator. To be able to correct for higher frequency fluctuations an EOM has been mounted inside the cavity as well. A tunable intra cavity glass plate mounted at Brewster angle allows the cavity length to be changed an thereby tune the laser frequency over range of 30 GHz [32] page 43 .

The major benefit with a dye laser is the wide frequency range it offers, the model used in this laser system can be tuned between 540 nm and 1040 nm by changing the dye in the system. The drawback is that the dye laser system often need quite a lot of maintenance to function properly.

4.3 Laser frequency stabilization system

The frequency stabilization is done using the PDH scheme previously described on page 3. The Fabry-Pérot cavity (B7600) is used as the reference and an EOM (B1800) is used to modulate the light before the cavity to create the frequency sidebands needed for the PDH locking. To measure the frequency of the light reflected from the cavity a photo diode is used (B7400).

Most of the electronics needed were in place before this master thesis started and will therefore not be described here, more information on these components can be found in [32].

4.3.1 Fabry Perot Cavity, B7600

The Fabry-Pérot cavity used was manufactured by Advanced thin films. The spherical spacer is made of ULE, it has one hole drilled thorough it for the laser light to pass and one hole for pumping the volume created by the spacer itself and the mirrors. The mirror substrates are made of fused silica and they are fitted with ULE compensation rings on the backside to minimize cavity length changes due to thermal fluctuations. The cavity has a finesse $< 150\ 000$ in the wavelength range 580nm - 606nm. Detailed drawings of the cavity and the holder can be found in appendix A

Coupling light to the cavity

To efficiently couple light to the cavity the incident wavefront has to have the same vergence as the cavity mode. A lens is used to focus the light beam incident on the cavity. To determine the focal length and position of the lens simulations were done using ABCD transfer, see appendix C for the octave code used for the simulations, [14] page 777. See figure 4.3 for the calculated results.

Cavity holder

The holder for the cavity was machined out of Invar which is nickel-iron alloy with a very low thermal expansion (1.3ppm/K) in the temperature range where it will be used [33]. The holder consists of three parts, one bottom and two arms which are fixed with screws to the bottom part, see figure 4.4. The arms are adjustable in height and the surfaces of the arms and the surfaces of the bottom part where the parts are in contact are slightly tilted compared to the translation direction. This means that when the arms are adjusted in height the distance between them change and thereby the pressure that will be applied to the cavity when it's mounted. See appendix A for detailed drawings of the holder.

Cavity mounting procedure

A lot of effort was put into mounting the cavity at the correct "squeeze insensitive" angle previously discussed. Calculations and measurements done

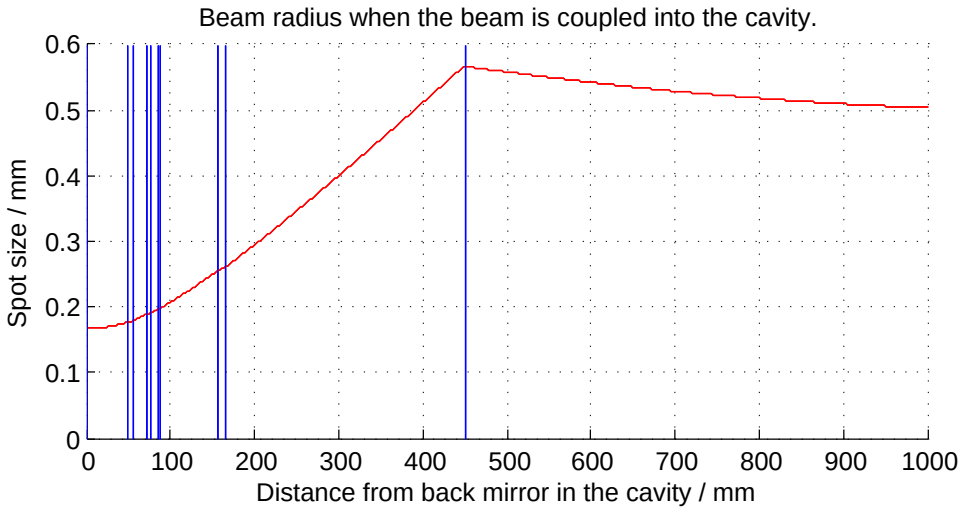

Figure 4.3: Beam radius when the beam is coupled to the cavity, calculations done using ABCD matrices. The vertical lines indicate surfaces. From right to left the lines are positive lens (f=430mm), viewport in vacuum chamber, two isolating windows in the heat shields and finally the cavity mirrors.

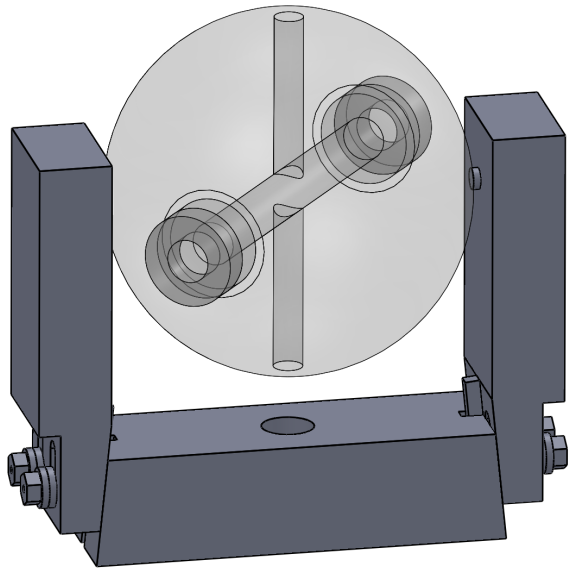

Figure 4.4: Invar cavity holder with cavity mounted.

for the type of cavity used in the stabilization system suggests that the angle between the optical axis and the mounting angle should be correct within a 0.1^0 not to ruin the ultimate stability [20]. This corresponds to mounting the cavity in the correct position within approximately 50 μm.

Firstly the holder was placed on a rotational stage, by measuring light intensity of a laser beam that was partly blocked by a screw mounted exactly in the middle of the holder it could be centered on the rotational stage. Three micrometer screws were mounted on the rotational stage with special holders. The cavity it self was then placed on the micrometer screws, the micrometer screws could then be used to adjust the position of the cavity in all three translational directions. By rotating the stage the angle between the optical axis and the mounting axis could be measured. Once the cavity was in the right position the arms on cavity holder were mounted which then secured the cavity in the correct position. Small viton o-rings (outer diameter 6.35 mm) were placed between the holder arms and the cavity.

4.4 Frequency shifter AOM

Once the cavity has been temperature stabilized the transmission spectrum of the cavity will be fixed in frequency and the transmission fringes will have a spacing of roughly 3 GHz. For the frequency stabilization system to function the light sent to the cavity has to match the frequency of one of the transmission fringes.

This means that there has to be some ability in the system to shift the frequency of the light incident to the cavity. One possibility would be to use the frequency tuning ability of the dye laser but the laser will be used for spectroscopy measurements and then the freedom to tune the laser frequency in absolute terms is needed during the experiments. The solution is to use an AOM that only frequency shifts the light going to the frequency stabilization system.

In figure 4.5 a schematic sketch of the AOM setup can be seen. The AOM set up so the light passes it twice, this has the benefit that the direction of the light beam after the AOM doesn't change even if the driving frequency of the AOM changes. Seen from the top view the light beam incident hits the AOM crystal at an angle much large than the optimal bragg angle and the polarization of the light is orientated the wrong way, therefore no light is diffracted. Seen from the side the angle between the incident light beam and the crystal is optimized for maximum diffraction which means that between 10% and 20% of the light intensity will be diffracted, the amount depends on the driving frequency of the AOM.

The AOM used is from Brimrose, model GPF-1125-750-590 (B5200). It has a broad bandwidth (375-1875 MHz) but the diffraction efficiency is comparably low (10%-20% of the light intensity) [34]. In the worst case 1% of the incident light on the frequency shifter setup will be transmitted, this is enough for the application.

The active volume inside the AOM is quite small, around 380μm in the

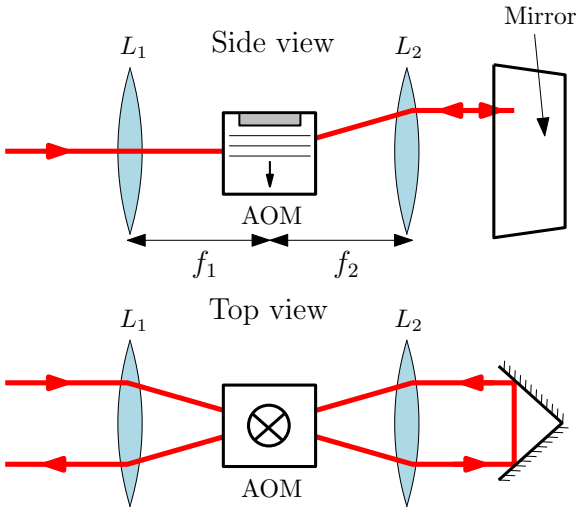

Figure 4.5: Double pass AOM setup.

direction of the laser beam and around $75\mu m$ wide [35]. This meant that some simulations were needed to determine the focal length and the position of the lens in front of the AOM to get the optimal spot size inside the AOM crystal.

4.5 Optical fiber with fiber noise cancellation

After passing the frequency shifter AOM (B5200) and some other components there is big risk that the beam profile have been distorted. To get one well shaped spatial mode the light is sent through a single mode fiber before it's coupled to the cavity. The fiber only supports the fundamental mode, all other modes will be heavily attenuated and thereby filtered out. The fiber used is 50 cm long and comes from Thorlabs, model PM460-HP-BK.

The optical fiber also comes in handy to couple light between the optical table and the active stabilization platform. The active stabilization platform will move to compensate for vibrations so if the light were sent through the air between one mirror on the optical table to a mirror on the stabilization platform the distance between them would shift when the stabilization platform moved. This would frequency modulate the light with the same frequency as of the mechanical vibrations the stabilization platform were compensating for.

The optical fiber will introduce phase noise on the light passing through it. The noise comes from movements in the fiber due to mechanical vibrations and length changes due to thermal fluctuations. Therefore a fiber noise cancellation system is needed to compensate for the noise, a system much like the one previously described on page 5 is used.

4.6 Laser intensity stabilization system

Some of the laser light sent into the cavity will be absorbed by the optical parts even if they are all anti reflex coated. This will lead to some heating of the cavity, to keep the heating constant the laser intensity is stabilized.

A photo diode (B7000) measuring the intensity is placed after the cavity, this will measure the amount of light intensity that couples to the cavity which is what should be measured to able to stabilize the light intensity inside the cavity. There is a intensity stabilization system for the main dye laser (B200) but this can't be used because it measures the light intensity directly after the dye jet laser and will not compensate for intensity changes due to for instance efficiency changes in the double pass AOM.

The power to the AOM used for fiber noise cancellation (B6500) is used to regulate the light intensity. By changing the power to the AOM the diffraction efficiency changes and thereby the light sent to the cavity.

4.7 Cameras for optical alignment

If a optical system is used during a long time (years) there will probably be changes done that requires that some of the optical components are re-aligned. To simplify that work three cameras have been put into the system at different positions. One camera (B7000) is placed behind the cavity to simplify the work of coupling light to the cavity and to be able to verify that the light couples to the right cavity mode.

The other two cameras are used to measure the direction and position of the beam from the dye laser. These two cameras are fitted with frosted glass windows and lenses that image the picture of these windows to the sensor. One camera (B5000) is placed close to laser to and the other (B5100) some distance away to be able to see how well collimated the beam is and detect any changes in angle. The cameras used are from Thorlabs, model DCC1545.

4.8 Temperature stabilization and thermal isolation

It's critical to maintain a stable temperature of the cavity to avoid changing the cavity length due to thermal expansion of the spacer material and mirror coatings. When the cavity is kept at the minimum expansion temperature it will probably have a sensitivity to temperature fluctuations in the order of 1-10 Hz/mK. For the cavity to have this relatively low sensitivity to thermal fluctuations it has to be kept at the minimum expansion temperature with a absolute precision of at least 0.1 K [19]. This are quite demanding requirements and are not completely trivial to meet.

The key components in the temperature stabilization system are the thermistor (B8000) measuring the temperature in a point near the cavity, a peltier element (B7900) to change the temperature and finally vacuum and heat shields to isolate the cavity from the environment. In addition to the specific temperature stabilization system used for the assembly inside the

vacuum chamber the whole lab where the laser system is places is temperature stabilized to a precision of 0.5K.

By placing the cavity in vacuum it is isolated from heat transfer by convection, the vacuum chamber basically works like an ideal thermo flask. The cavity can only be heated by radiation or through the mount holding it. Some of the laser light sent into the cavity will be absorbed by the optical parts.This will lead to some heating of the cavity, to keep the heating constant the laser intensity is stabilized.

4.8.1 Heat shields

To minimize changed in the heat transfered to the cavity by radiation from the surrounding vacuum chamber a three layer aluminum heat shield is placed between the vacuum chamber and the cavity itself, see figure 4.6. The heat shields are only connected to the vacuum chamber with four small screws and a peltier element.

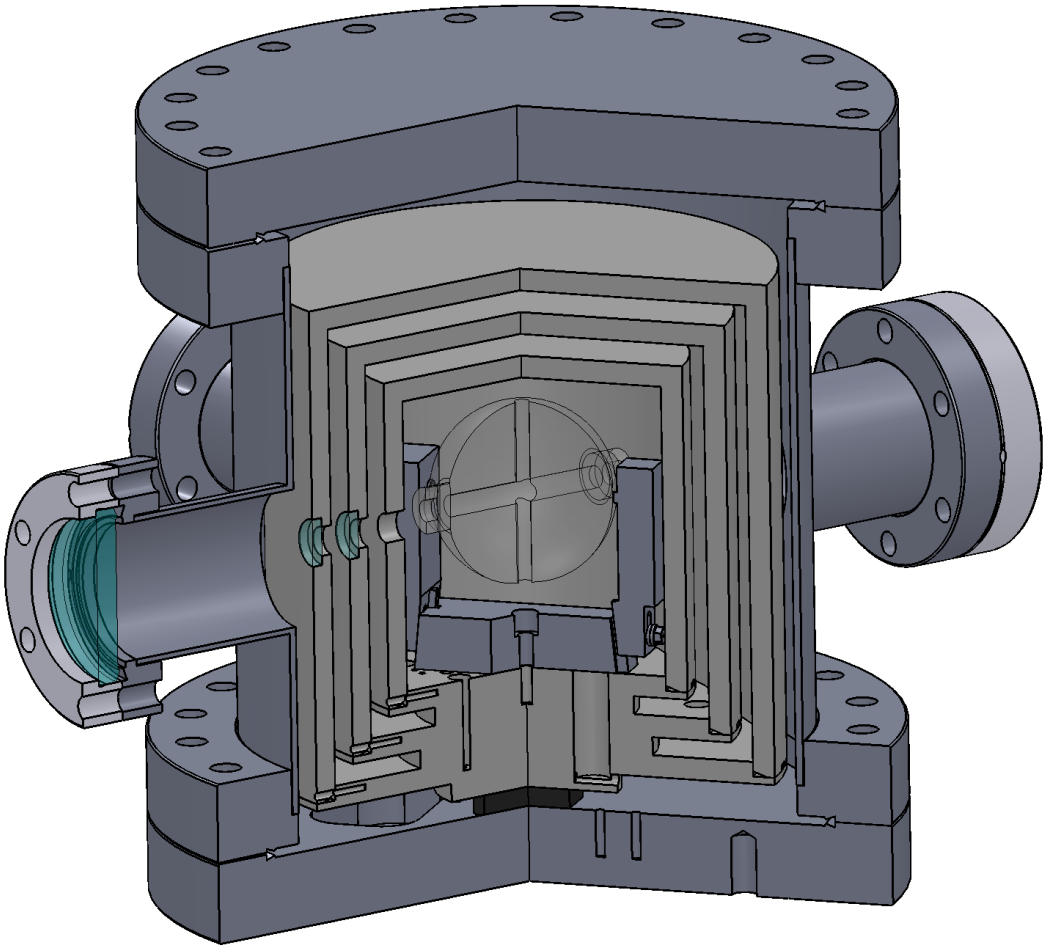

Figure 4.6: CAD model of the heat shields mounted inside the vacuum chamber. The heat shields are used to shield the cavity from fluctuations in the incident heat radiation.

When designing the heat shields FEM simulations were done to evaluate different geometries. The simulations were done using the software package Comsol. To allow the heat shields to be vacuum pumped holes were made. These were placed in the bottom part of the heat shields, close to the peltier element to allow the peltier element to compensate for the changes quicker. Detailed drawings of the heat shields can be found in appendix A.

4.8.2 Temperature control system

To stabilize the temperature a Thorlabs TED200 (B8100) temperature controller is used which is analog PID controller, with control precision of 3 mK in the range 0-20°C [36].This means that the temperature controller might be the limiting factor on the overall system performance when all other noise sources have been eliminated.

The temperature is measured with a EPOTEK model 871-B57560G203F thermistor (B8000) and the temperature is changed with a Custom Thermoelectrics model 01701-9L31-09B peltier element (B7900). The peltier is bakeable to 200°C and the model have previously been tried out in UHV applications with good results [37].

4.9 Vibration isolation

Vibrations of the cavity will couple to the light inside the cavity and thereby ruin the performance of the stabilization system. It's therefore important to insulate the cavity from mechanical vibrations. In figure 4.7 the key components of the vibrations insulation system are illustrated.

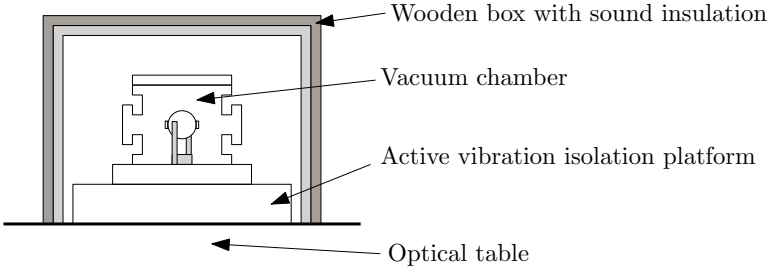

Figure 4.7: System overview

The whole setup is mounted on a floating optical table, model RS3000 from New Port. The vacuum chamber, with the cavity inside, is mounted on top of a active stabilization platform (B7800) which measures vibrations and actively compensate for them with piezo actuators. The platform used is from HWL Scientific instruments, model TS140LP.

The vacuum helps insulate the cavity from any acoustic vibrations that otherwise would have been coupled to the cavity through air. To further decrease the sensitivity to acoustic vibrations the setup is placed inside an wooden box lined with sound insulation foam. The shape of the cavity and

the way it's mounted is also very important to decrease the sensitivity to vibrations as previously discussed on page 13.

4.10 Vacuum system

Having the Fabry-Pérot cavity in vacuum serves three purposes. It significantly increases the thermal insulation of the cavity, it prevents acoustic vibrations from coupling to the cavity and the optical path length between the cavity mirrors doesn't fluctuate due to pressure variations. To keep the changes in optical path length due to pressure variations small enough not to ruin the stability of a 1 Hz laser the variations in pressure have to be kept $< 1 \times 10^{-8}$ mbar [19].

To be on the safe side the pressure inside the Fabry-Pérot cavity should be kept below 1×10^{-8} mbar. The use of heat shields inside the vacuum chamber further complicates things and due to the geometry of the heat shields they will probably give rise to a pressure gradient with a lower pressure next to the pump and a higher pressure inside the heat shields. Therefore the vacuum system has been designed to be at least one order of magnitude better than initially needed.

4.10.1 Equipment and setup

The setup of the vacuum system is rather straight forward, a diagram illustrating how all major components are connected can be seen in figure 4.8. The reference cavity is placed inside the vacuum chamber (2) which is connected to two pump set ups. The turbomolecular (6) pump with the diaphragm pump (7) installed as backing pump is used for pumping down the vacuum system from atmospheric pressure to 1×10^{-6} mbar. When the pressure is low enough the angle valve (3) is closed and the ion pump is started (1). All components used in the vacuum system except the roughing components (turbo pump, diaphragm pump and pressure gauge) are connected with CF flanges.

Table 4.3: Vacuum system components, numbering the same as used in figure 4.8.

Nbr	**Description**	**Manufacturer**	**Model**
1	Ion pump	Gamma vacuum	25S
2	Vacuum chamber	Vacom	Custom design
3	Angle valve	VAT	28432-GE01
4	Flexible hose	Vacom	FX40CF75R-304
5	Pressure gauge	Pfeiffer	PKR 251
6	Turbo molecular pump	Pfeiffer	HiPace 80
7	Diaphragm pump	Pfeiffer	MVP 015

The vacuum chamber used was custom made for this application, the chamber can be seen in figure 4.9. It's equipped with four CF40 flanges,

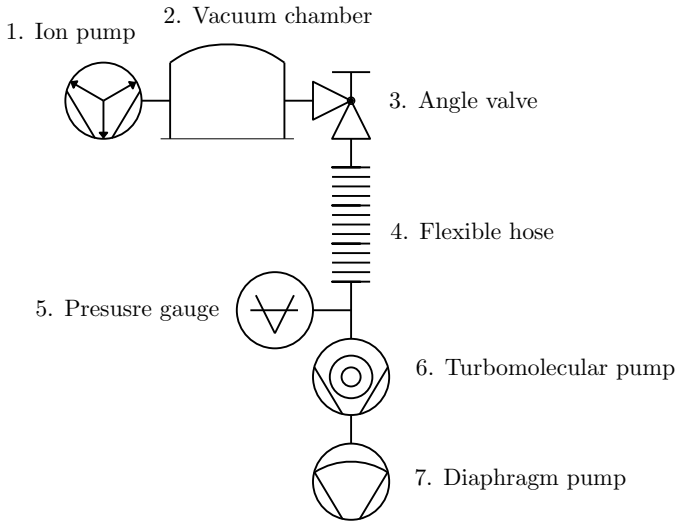

Figure 4.8: Schematic over the vacuum system used in the stabilization system. See table 4.3 for more details on the components used.

two used to connect the vacuum pumps and two used for coupling light into the cavity. The chamber also has two CF160 flanges, the top one is fitted with a blind flange and the bottom one is fitted with a flange with a eight pin dsub connector feed through. The electrical feed through is used for connecting the peltier element and thermistor inside the vacuum chamber with the temperature control system. Detailed drawing of these parts can be found in appendix A.

Vacuum pumps

In the stabilization system a Pfeiffer HiPace 80 turbomolecular pump (6) is with a Pfeiffer MVP01 diaphragm pump (7) as fore vacuum pump is used for rough pumping. The turbomolecular pump has a ultimate pressure $< 1 \times 10^{-7}$ mbar. The turbo pump is unsuitable to use during operation of the stabilization system due to the vibrations that might couple from the pump to the rest of the system.

The ion pump (1) used is a Gamma vacuum 25S with DI elements, which is equipped with both titanium and tantalum elements. The ion pump is suitable for this application for a number of reasons, it has no moving parts which means that it will not introduce any vibrations to the system, it has a low ultimate pressure that will allow us to reach the required ultra high vacuum and it has a relatively long lifetime if not run at too high pressures. At delivery the ion pump used in the system could produce a vacuum of 3.1×10^{-11} when fitted with a blind flange. For low pressures the ion pump is used as a pressure gauge, the pressure is calculated by measuring the current needed to drive the ion pump.

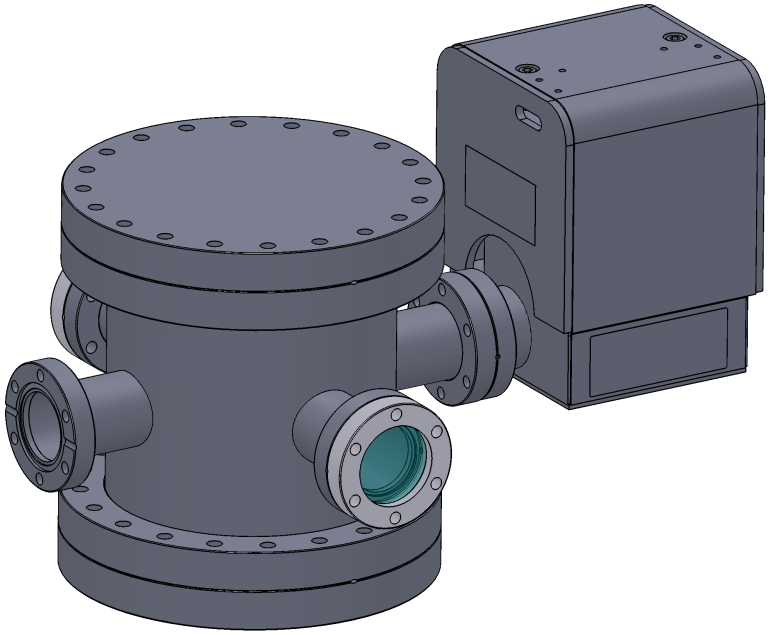

Figure 4.9: CAD model of the vacuum chamber used in the vacuum system. In the picture the ion pump is mounted as well as the viewports but not the turbomolecular pump.

4.10.2 Vacuum practice

When designing and assembling UHV systems there are some things that needs to be considered to be able to attain the desired vacuum. The things are not very complicated to avoid but missing out on just one thing can potentially mean completely ruining the vacuum.

Materials

Not all materials are suitable for use in UHV applications. Materials used should have low outgassing i.e. the amount of gas released from the material should be low not to compromise the vacuum. The molecules gassing out can come from the material itself or be molecules previously bounded to the material by some chemical process. NASA maintain a list of low outgassing materials that can be useful when selecting materials to use in vacuum applications [38].

In the process of pumping down a vacuum system it is common practice to bake it, this a process where the system is heated to get rid of contaminations. The baking process will be further discussed on page 36. Materials used for UHV applications should therefore be able to withstand a temperature of at least 200°C over an extended period of time. In the stabilization system all components used in the vacuum chamber, except the Fabry-Pérot cavity (B7600), are specified to withstand a temperature of 200°C.

Handling and cleaning

Care has to be taken not to introduce any contaminations into the vacuum system. This means proper cleaning of all components and handling all components with care not to contaminate them. A single fingerprint on a surface can easily ruin the vacuum. During the construction work all vacuum components were only handled using Kim Clark Purple Nitrle Gloves [39].

There are no generic cleaning methods applicable for all cases, depending on what vacuum performance needed and which materials used that are used different cleaning procedures have to be employed. Sometimes the type of machining technique used to manufacture the part might also play a difference. Some of the parts used in the vacuum system were bought cleaned and ready to use while other parts machined in the local workshop had to be cleaned. All minor parts going into the vacuum chamber were cleaned with ethanol in a ultra sonic bath [40]. The larger alumina heat shields were cleaned in a warm, high pH bath, much like a ordinary dishwasher. To verify that the cleaning procedure worked properly all major components were put into the chamber and a trial pump done was done. The cleaning procedures used turned out to be sufficient and it was possible to reach the desired pressure, see figure 4.11 for pressure curves.

Gas flow

In ultra high vacuum (UHV), pressure ranges of around 1×10^{-7} mbar and lower, there are so few molecules that the interaction between them can be neglected [28] page 33. This pressure regime is referred to as the molecular flow regime. When the molecules don't interact with each other they behave much like photons. This imposed somewhat of a problem when the heat shields were designed because they should allow good pumping but at the same time shield the cavity from heat photons. The solution to this problem was to design good heat shields in the sense of heat insulation and then design the vacuum system to be one or two orders of magnitude better then needed. The better performance of the vacuum system can then compensate for the pressure gradient created by the heat shields.

The risk of trapping gas in pockets also has to be accounted for, if it happens the gas will slowly leak out from the pocket over time and thereby ruin the vacuum. A typical pitfall is when screws are used, a gas pocket will always be created below the screw if the hole where the screw is fitted is unventilated. To avoid this ventilated screws have to be used, these are screws with a center hole or a slot running down the side of the screw to allow trapped gas to escape, see figure 4.10.

Baking of vacuum systems

When vacuum components are exposed to the atmosphere different gas molecules will be absorbed in the surfaces of the equipment. When the vacuum system then is pumped down these molecules will be deabsorbed over time. This outgassing will prolong the time it takes to pump down a

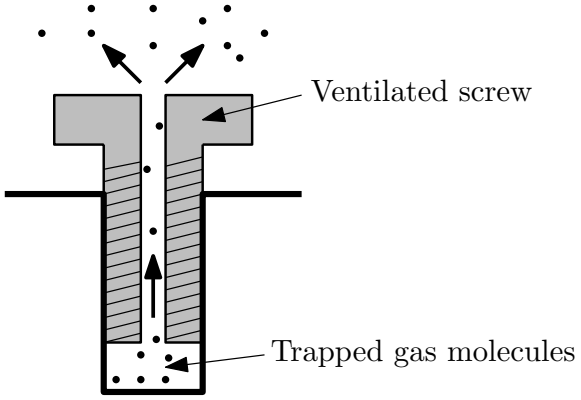

Figure 4.10: The cross section of a center ventilated screw, the center hole allows trapped gas to be easily pumped.

system and limit the ultimate pressure. To shorten pump down times the vacuum system is usually baked, this is a process during which the vacuum system is heated to make molecules trapped in the surfaces gas out quicker.

To reach pressures in the range of 1×10^{-10} mbar a system should be heated to at least 120°C during a minimum of 48 hours, [28] page 49. A trial pump down of the system was carried out to make sure all vacuum components worked as expected. The pump down was made without any optics mounted inside the chamber. The baking was carried out over one and half week and the final pressure reached after baking was around 2×10^{-10} mbar. The measured pressure and outside temperature of the chamber can be seen in figure 4.11. The speed of the temperature increase when baking the system should be well below 3°C/min not to damage the viewports [41]. To get a even temperature over the complete vacuum system it was wrapped in glass fiber blanket and alumina foil.

To be able to mount the optical components inside the chamber it had to be opened and thereby exposed to the atmosphere. This meant that the surfaces became contaminated and therefore a new bake out of the system had to be carried out. The Fabry-Pérot cavity is sensitive to prolonged heat exposure, there is a risk that the optical contacting bonding the mirrors to the spacer will crystallize [42]. This would make it impossible to change the cavity mirrors and therefore the complete cavity would be rendered useless if a mirrors was contaminated. The measured pressure in the chamber and the temperature during the second bake out can be seen in figure 4.12.

By comparing the two figures, 4.11 and 4.12, it's quite evident that baking of the system for a longer time is of paramount importance to achieve low pressures. When baking the system the first time, for more than a week, a pressure two orders of magnitude lower was reached compared to the second bake out which was done at a lower temperature during one day only. There can also be other reasons for this such as contamination on the optical components that were added before the second bake out.

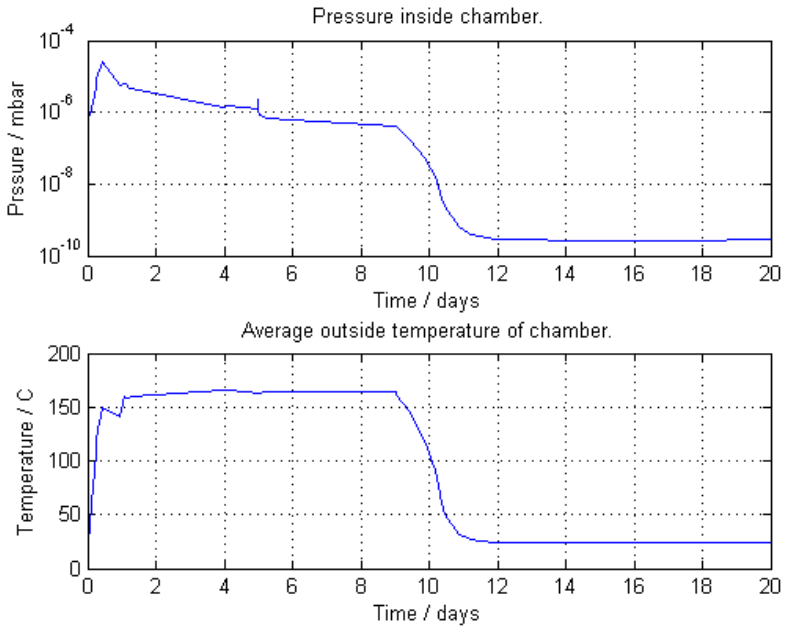

Figure 4.11: Pressure curve and temperature curve when the first proper baking of the vacuum system was done. The temperature is an average from four different sensors placed on the outside of the vacuum chamber.

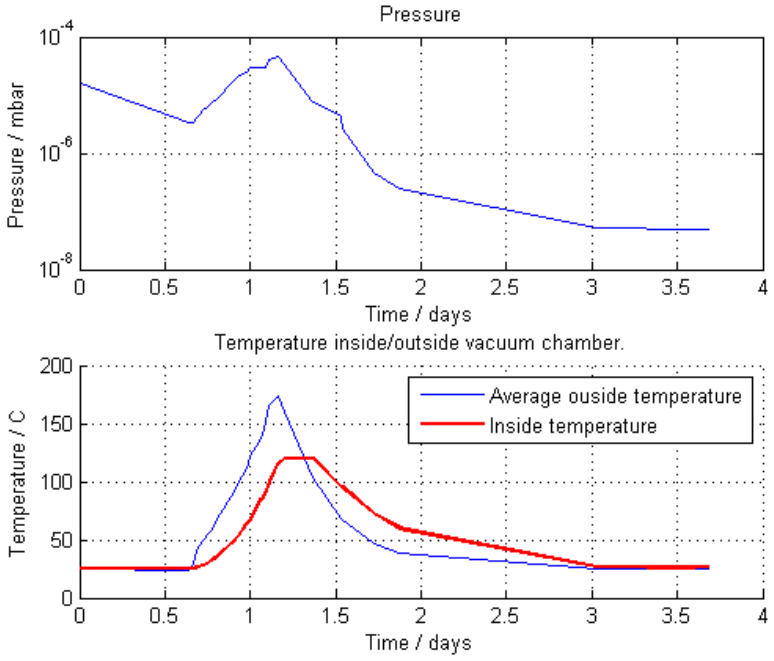

Figure 4.12: Pressure curve and temperature curve when baking the vacuum system with the full optical setup inside the chamber. 45 days after the baking was done the pressure had dropped to 8.2×10^{-10} mbar.

5 Roadmap to 2 Hz stability

Some work remain before the stabilization system will be operational. In this chapter a outline is given over what has to be done to achieve the desired 2 Hz stability.

5.1 Current status of the system

As the system stands today all optical components have been assembled and roughly aligned. Most of the electronics are also assembled but some work remains, especially with the electronics for the fiber noise cancellation system. In addition to this the Fabry-Pérot cavity's minimum expansion temperature has to be determined as well to get the desired low sensitivity to thermal fluctuations.

5.2 Frequency shifter AOM and optical alignment

At the moment there are some unresolved problems in conjunction to the frequency shifter AOM (B5200). When the driving frequency changes the angle of the diffracted laser beam changes and thereby also the point where the beam hits the second lens (L_2 in figure 4.5). Due to spherical aberrations in the lens the focal length varies slightly depending on where on the lens the laser beam hits. This means that the focus of the beam on the second pass through the AOM will be shifted. This cause some problems because the shift is big enough to move the focus outside the active volume of the AOM. The shift can probably be compensated for by using an aberration free lens but some simulations are needed to ensure that it's the most suitable solution.

When the frequency shifter AOM is operational all optical components have to be properly aligned, both on the optical table and on the vibration isolation platform. Light can then be coupled to the cavity and the laser intensity stabilization system and the frequency stabilization system can be tried out.

5.3 Fiber noise cancellation

The fiber noise cancellation system for the fiber connecting the optical table with the vibration stabilization platform is not yet finished. All optical components are in place but the electronics are not yet constructed. As mentioned earlier the specifications for the frequency stability of the signals used in the fiber noise cancellation system are quite strict and some time will have to be invested if the electronics are to be designed. An alternative would be to buy some signal generators that fulfill the specifications but these tend to be quite expensive compared to the cost of designing the electronics on your own.

In the current setup the dye laser system is located on one table and the experimental setup on an other, a fiber is used to couple the light between the two tables. That fiber will also need a fiber noise cancellation system before it's possible to use the frequency stable light in any experiment, it's worth keeping in mind when designing and buying equipment for the first fiber noise cancellation system.

5.3.1 Signal generating electronics, B6200

An alternative to buying very expensive signal generators is to build the needed electronics yourself. A rough outline of such a system is given in figure 5.1

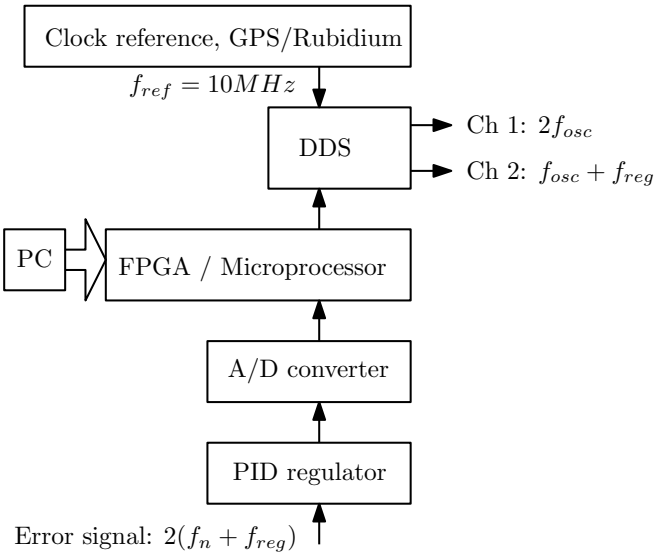

Figure 5.1: Possible design of frequency generation circuitry for fiber noise cancellation system. See table 5.1 for more details on suitable components.

A direct digital synthesizer, DDS, can be used to generate the signals. To get the frequency stability needed the DDS has to locked to some reference oscillator . One of the signals generated by the DDS should be tunable. This can be done by digitizing the analog error signal from the PID regulator (B6000) and using it to control the frequency offset of the tunable signal. To

Table 5.1: Proposition on components that might be useful for the frequency generation circuitry needed for the fiber noise cancellation system. There are probably better components but this gives a hint where to start looking.

Component	**Manufacturer**	**Model**
Rubidium frequency standard	Stanford Research Systems	FS725
DDS	Analog devices	AD9910
Rubidium frequency standard	Stanford Research Systems	FS725
FPGA	Altera / Xilinx	-
A/D converter	Analog devices	-

create an interface between the A/D converter and the DDS some digital circuitry is needed as welll, a microprocessor or field programmable gate array, FPGA would probably work. This circuit would also work as an interface between a PC and the DDS to enable the frequencies to be controlled by some PC software.

An alternative to using a DDS is using voltage controlled oscillators, VCOs, the drawback is that they are fixed at one center frequency with a very limited pulling range, typically < 100 ppm. This means that one oscillator at the optimal working frequency for the AOM (around 60 MHz) and one VCO at exactly the double frequency of the first on is needed.

Previous measurements on the phase noise introduced by the fiber connecting the laser system with the experimental setup indicates that the maximum phase drift is in the order of $5°/20\mu s$. This means that the control system for the fiber noise cancellation needs a bandwidth of at least 1 kHz. The AOM (B6500) and the regulator (B6900) used more than well meet that requirement. The electronics constructed have to do that as well.

5.4 Determine minimum expansion temperature

The spacer in the Fabry-Pérot cavity is made of ULE glass. As previously mentioned ULE glass has a minimum expansion temperature at which the cavity length will be the least sensitive to thermal fluctuations. The minimum expansion temperature is determined by a number of factors such as different manufacturing batches of ULE glass, the dimensions and material of the mirror substrates and the dimensions of the compensation rings attached the backside of the cavity mirrors. This means that measurements of the minimum expansion temperature has to be done for every type of cavity and for each batch of ULE glass.

The minimum expansion temperature is found by changing the temperature of the cavity while the stability of the laser is measured. This means that some kind of reference is needed for the measurement of the frequency stability. Ideally the reference would be a second ultra stable laser but in absence of such a spectral hole in a Europium doped crystal could be used as a reference instead.

An alternative to doing the measurements yourself is to buy the information from the company that have manufactured the cavity. The have done measurements on the same type of cavity made from the same batch of ULE.

Acknowledgments

I would like to thank Lars Rippe and Stefen Kröll for the opportunity to do my master thesis in the quantum information group at the atomic physics division at Lund University. I couldn't wish for a better supervisor than Lars, we have had a ton of fun together and I have learned a lot useful things on the way.

It have been a very fun and worthwhile time being part of the quantum information group. I would like to thank the rest of the group with Jenny, Yen and Mahmood for the support they have given me. There have always been someone to answer my questions and to have a cup of coffee with.

Janis Alnis at the Max Planck institute in Münich was a great support in the first phase of the thesis when the system was designed. He invited us to visit the lab where he works and demonstrated the frequency stabilization systems he had designed and built. Jörgen Larsson at the Atomic physics division opened the contact to MAX-lab and helped us with some vacuum equipment. Anders Månsson at MAX-lab was a great source of information about handling and cleaning vacuum equipment. He also provided help with cleaning some of major vacuum components.

Göran Petterson working in the workshop at the Physics department provided valuable input during the design of the heat shields and then did the actual machining of the heat shields. Mathieu Gisselbrecht working at the Synchrotron Radiation division helped during the design process of the vacuum system and provided some equipment of crucial importance for baking of the vacuum system.

Bibliography

[1] T. H. Maiman. Stimulated optical radiation in ruby. *Nature*, 187:493–, 1960.

[2] T. Rosenband, D. B. Hume, P. O. Schmidt, C. W. Chou, A. Brusch, L. Lorini, W. H. Oskay, R. E. Drullinger, T. M. Fortier, J. E. Stalnaker, S. A. Diddams, W. C. Swann, N. R. Newbury, W. M. Itano, D. J. Wineland, and J. C. Bergquist. Frequency ratio of al+ and hg+ single-ion optical clocks; metrology at the 17th decimal place. *Science*, 319(5871):1808–1812, March 2008.

[3] NIST. The nist reference on constants, units, and uncertainty. http://physics.nist.gov/cuu/Units/second.html, August 2011.

[4] Thomas E Parker. Long term comparison of caesium fountain primary frequency standards. *Metrologia*, 47:1–10, 2010.

[5] C. W. Chou, D. B. Hume, J. C. J. Koelemeij, D. J. Wineland, and T. Rosenband. Frequency comparison of two high-accuracy al+ optical clocks. *Physical Review Letters*, 104(7):070802, February 2010.

[6] R. W. Equall, R. L. Cone, and R. M. Macfarlane. Homogeneous broadening and hyperfine structure of optical transitions in pr/sup 3+/:y/sub 2/sio/sub 5/. *Phys. Rev. B*, 52:3963–3969, 1995.

[7] R. W. P. Drever, J. L. Hall, F. V. Kowalski, J. Hough, G. M. Ford, A. J. Munley, and H. Ward. Laser phase and frequency stabilization using an optical- resonator. *Appl. Phys. B*, 31(2):97–105, 1983.

[8] E. D. Black. An introduction to pound-drever-hall laser frequency stabilization. *Am. J. Phys.*, 69(1):79–87, 2001.

[9] L. S. MA, P. JUNGNER, J. YE, and J. L. HALL. Delivering the same optical frequency at 2 places - accurate cancellation of phase noise introduced by an optical-fiber or other time-varying path. *Optics Letters*, 19(21):1777–1779, 1994.

[10] W.J. Riley. *NIST Special Publication 1065, Handbook of Frequency Stability Analysis*. NIST, July 2008.

[11] David W. Allan. Statistics of atomic frequency standards. *Proceedings Of The IEEE*, 54:221–230, 1966.

[12] M.C. Teich B.E.A. Saleh. *Fundamentals of Photonics*. Wiley, 2007.

[13] Eugene Hecht. *Optics*. Addison-Wesley, 2002.

[14] A. E. Siegman. *Lasers*. University science books, 1986.

[15] D. Z. Anderson, J. C. Frisch, and C. S. Masser. Mirror reflectometer based on optical cavity decay time. *Applied Optics*, 23(8):1238–1245, 1984.

[16] H. B. Callen and R. F. Greene. On a theorem of irreversible thermodynamics. *Physical Review*, 86(5):702–710, 1952.

[17] K. Numata, A. Kemery, and J. Camp. Thermal-noise limit in the frequency stabilization of lasers with rigid cavities. *Phys. Rev. Lett.*, 93(25):250602, December 2004.

[18] A. D. Ludlow, X. Huang, M. Notcutt, T. Zanon-Willette, S. M. Foreman, M. M. Boyd, S. Blatt, and J. Ye. Compact, thermal-noise-limited optical cavity for diode laser stabilization at 1 x 10(-15). *Opt. Lett.*, 32(6):641–643, March 2007.

[19] J. Alnis, A. Matveev, N. Kolachevsky, T. Udem, and T. W. Hansch. Subhertz linewidth diode lasers by stabilization to vibrationally and thermally compensated ultralow-expansion glass fabry-perot cavities. *Physical Review A*, 77(5):053809, May 2008.

[20] Mark Notcutt Robert E. Drullinger Till Rosenband James C. Bergquis David R. Leibrandt, Michael J. Thorpe. Spherical reference cavities for frequency stabilization of lasers in non-laboratory environments. *Optics Express*, 19:3471–3482, 2011.

[21] Corning. Corning ultra low expansion glass, ule, code 7972. Technical report, Corning, 2011.

[22] T. Legero, T. Kessler, and U. Sterr. Tuning the thermal expansion properties of optical reference cavities with fused silica mirrors. *Journal of the Optical Society of America B-optical Physics*, 27(5):914–919, May 2010.

[23] M. Notcutt, L. S. Ma, J. Ye, and J. L. Hall. Simple and compact 1-hz laser system via an improved mounting configuration of a reference cavity. *Opt. Lett.*, 30(14):1815–1817, July 2005.

[24] H.J. Goldsmid G.S. Nolas, J. Sharp. *Thermoelectrics Basic Principles and New Materials Development*. Springer-Verlag, 2001.

[25] Custom Thermoelectrics. Peltier device do's and don'ts. Technical report, 2011.

[26] Kurt J. Lesker Company. *Technical Note, Flange system overview.*

[27] MDC Caburn Europe. *Caburn MDC Vacuum Catalog, page 8.*

[28] Pfeiffer. *Vacuum Technology Know How.* Pfeiffer Vacuum, 2010.

[29] L. Schulz. Sputter-ion pumps. Technical report, Paul Scherrer Institut.

[30] B. C. Young, F. C. Cruz, W. M. Itano, and J. C. Bergquist. Visible lasers with subhertz linewidths. *Phys. Rev. Lett.*, 82(19):3799–3802, May 1999.

[31] J. Helmcke U. Sterr H. Stoehr, F. Mensing. Diode laser with 1 hz linewidth. *Optics letters*, 31:736 – 738, 2006.

[32] L. Rippe. *Quantum Computing with Naturally Tapped Sub-Nanometre-Spaced Ions*. PhD thesis, Division of Atomic Physics, LTH, December 2006.

[33] Datasheet, Special Metals, The NILO and NILOMAG Nickel-Iron Alloys, 2011.

[34] Datasheet, Brimrose GPF-1125-750-590, 2011.

[35] Carla Green Brimrose. Mail communication, 2011.

[36] Datasheet, Thorlabs TED200, 2003.

[37] Andrew E. Masters Custom Thermoelectrics. Mail communication, 2011.

[38] NASA. Outgassing data for selecting spacecraft materials online. Technical report, http://outgassing.nasa.gov/, 2011.

[39] A. Tankut K.E. Miller, J.A. Grossnickle. Uhv cleaning technique and large high temperature uhv quartz to metal seal development for the tcs upgrade. Technical report, Redmond Plasma Physics Laboratory, University of Washington, Seattle, 2005.

[40] Anders Mansson MAX-Lab. Personal communication, 2011.

[41] Ian McGlashan Torr Scientific. Mail communication, 2011.

[42] Scot Davidson Advanced thin films. Mail communication, 2011.

A
Drawings

In this appendix drawings are provided of some of the mechanical parts used in the stabilization system. Drawings are only provided for the parts that are custom made for the system, please visit the homepage of the different manufacturers for detailed drawings of all standard components.

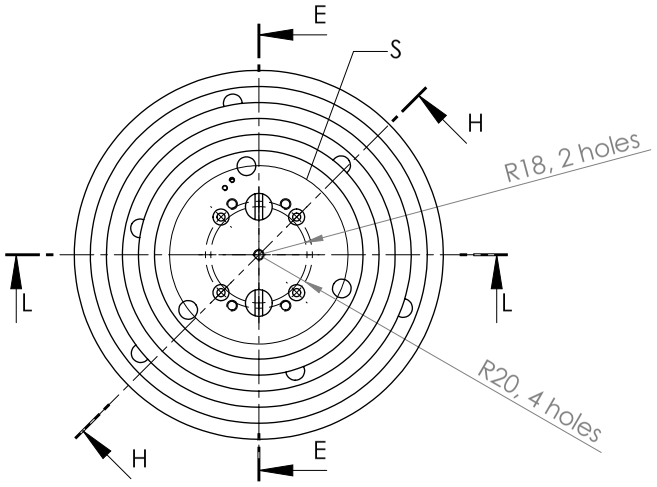

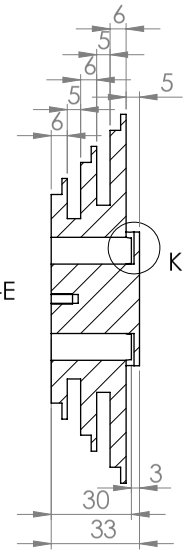

SECTION E-E

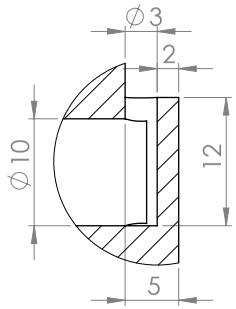

DETAIL K
SCALE 2 : 1

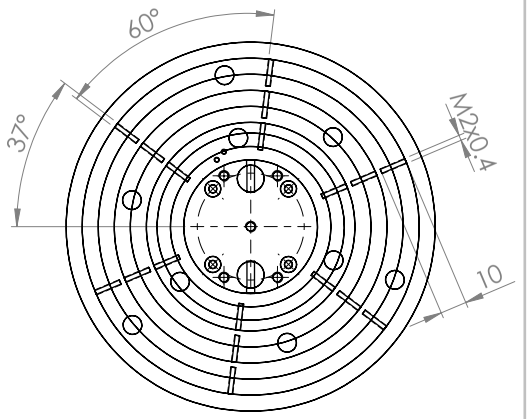

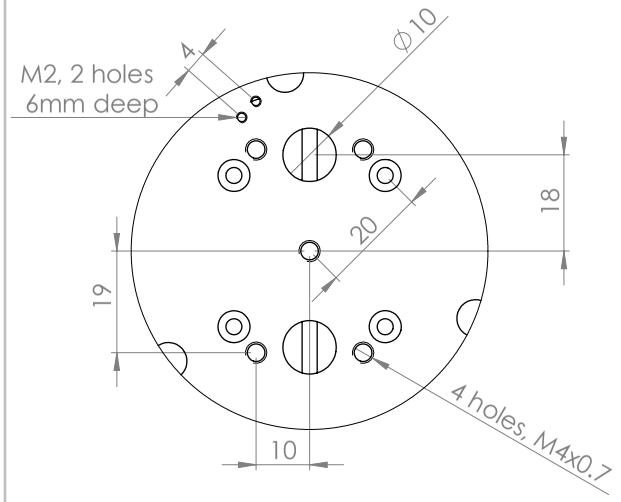

DETAIL S
SCALE 1 : 1

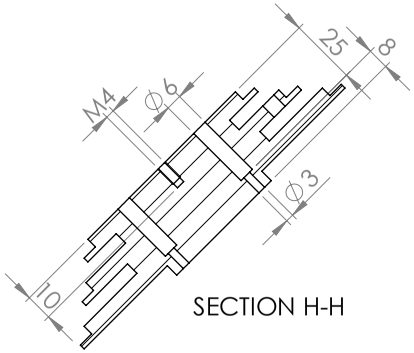

SECTION H-H

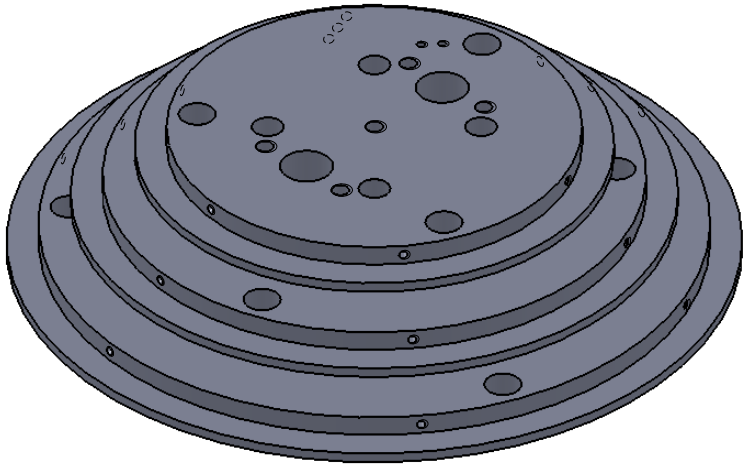

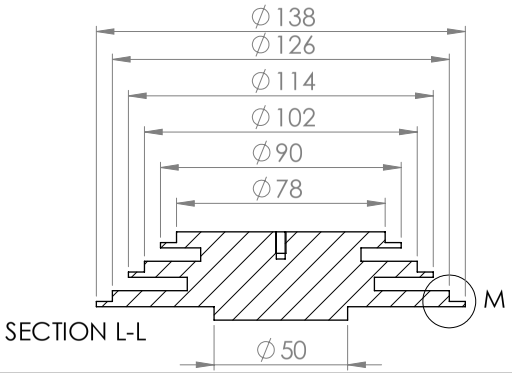

SECTION L-L

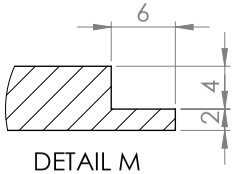

DETAIL M
SCALE 2 : 1

UNLESS OTHERWISE SPECIFIED: DIMENSIONS ARE IN MILLIMETERS SURFACE FINISH: TOLERANCES: LINEAR: ANGULAR:		FINISH:		DEBUR AND BREAK SHARP EDGES	DO NOT SCALE DRAWING	REVISION
	NAME	SIGNATURE	DATE		TITLE:	
DRAWN						
CHK'D						
APPV'D						
MFG						
Q.A				MATERIAL:	DWG NO.	A3
					Heat shield bottom	
				WEIGHT:	SCALE:1:2	SHEET 1 OF 1

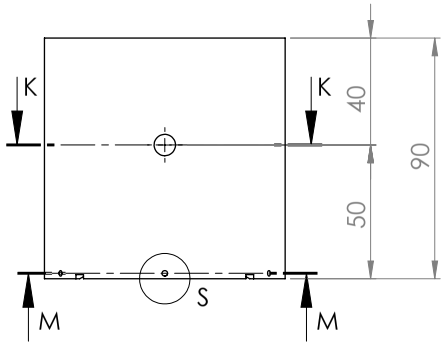

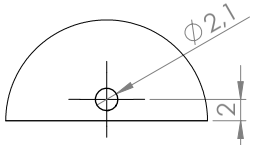

DETAIL S
SCALE 2 : 1

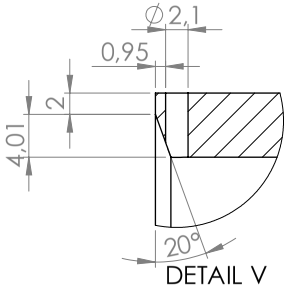

DETAIL V
SCALE 2 : 1

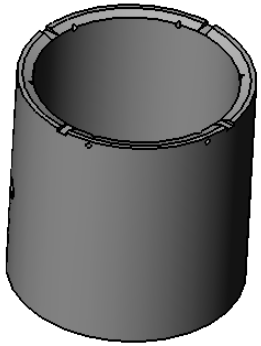

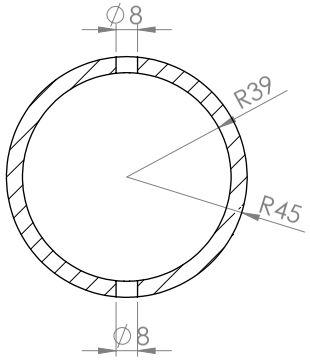

SECTION K-K

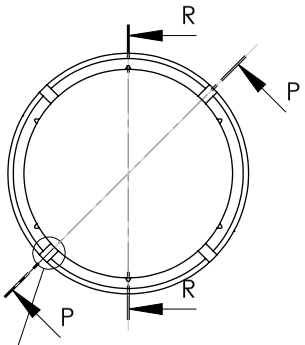

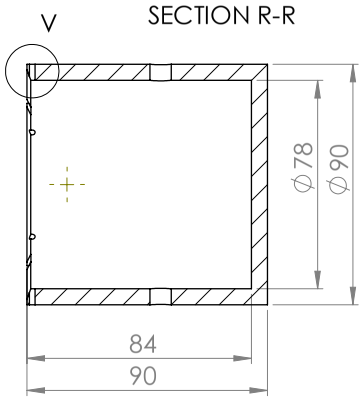

SECTION R-R

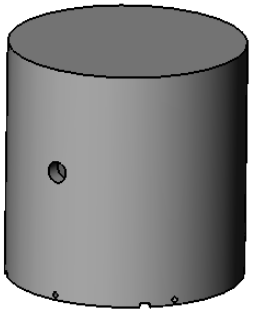

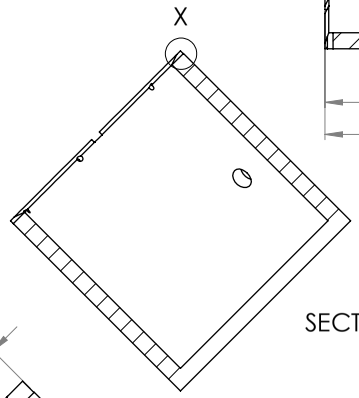

SECTION P-P

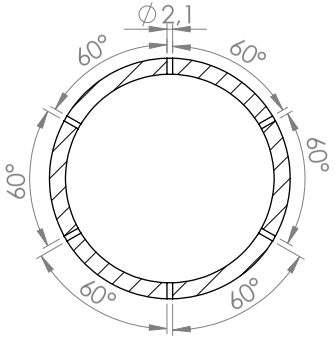

SECTION M-M

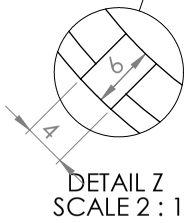

DETAIL Z
SCALE 2 : 1

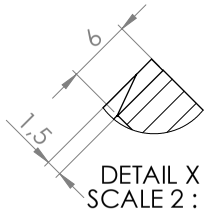

DETAIL X
SCALE 2 : 1

UNLESS OTHERWISE SPECIFIED: DIMENSIONS ARE IN MILLIMETERS SURFACE FINISH: TOLERANCES: LINEAR: ANGULAR:	FINISH:		DEBUR AND BREAK SHARP EDGES	DO NOT SCALE DRAWING	REVISION	
	NAME	SIGNATURE	DATE	TITLE:		
DRAWN						
CHK'D						
APPV'D						
MFG						
Q.A				MATERIAL:	DWG NO. Heat shield inner	A3
				WEIGHT:	SCALE:1:2	SHEET 1 OF 1

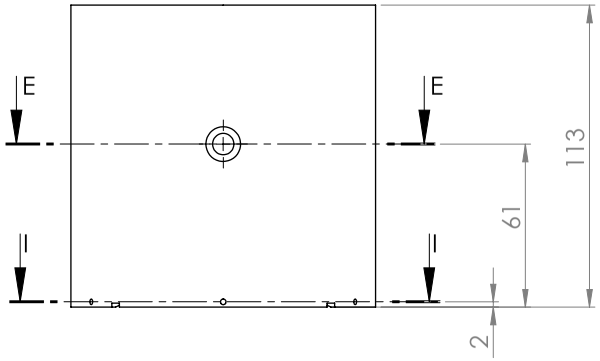

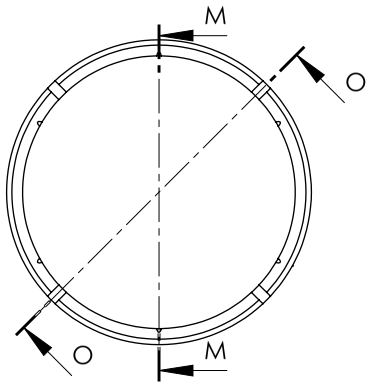

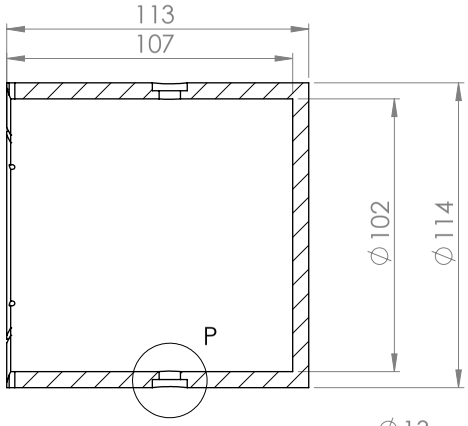

SECTION M-M

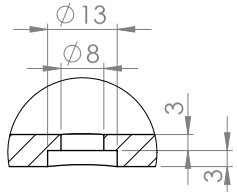

DETAIL P
SCALE 1 : 1

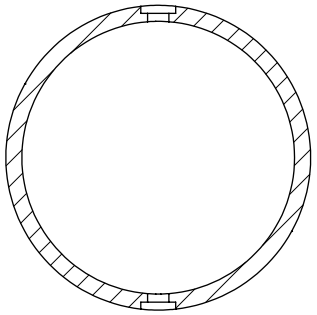

SECTION E-E

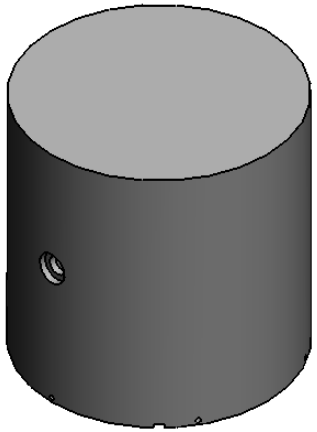

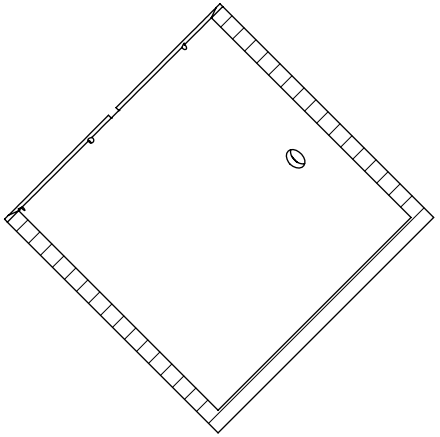

SECTION O-O

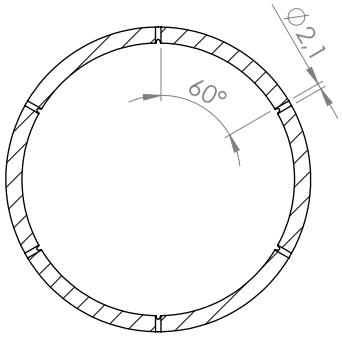

SECTION I-I

UNLESS OTHERWISE SPECIFIED: DIMENSIONS ARE IN MILLIMETERS SURFACE FINISH: TOLERANCES: LINEAR: ANGULAR:		FINISH:		DEBUR AND BREAK SHARP EDGES	DO NOT SCALE DRAWING	REVISION
	NAME	SIGNATURE	DATE		TITLE:	
DRAWN						
CHK'D						
APPV'D						
MFG						
Q.A				MATERIAL:	DWG NO. Heat shield middle	A3
				WEIGHT:	SCALE:1:2	SHEET 1 OF 1

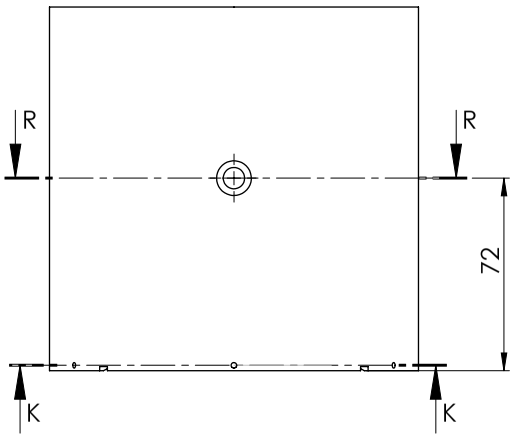

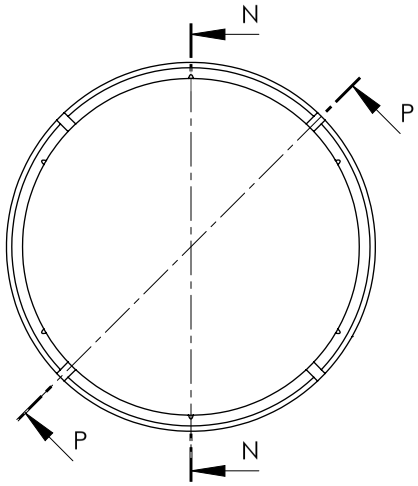

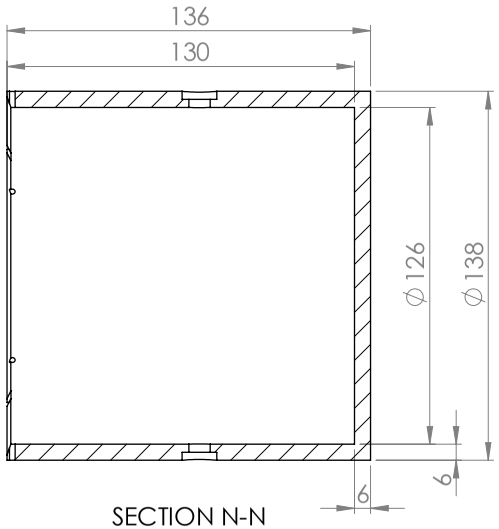

SECTION N-N

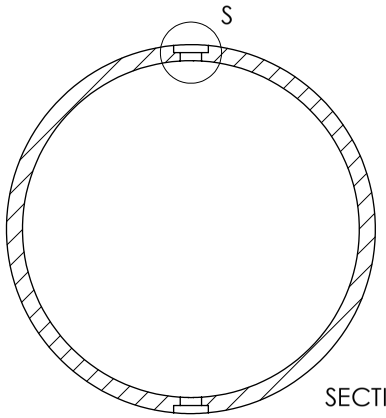

SECTION R-R

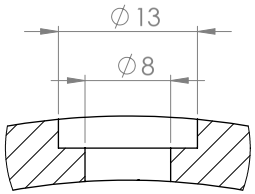

DETAIL S
SCALE 2 : 1

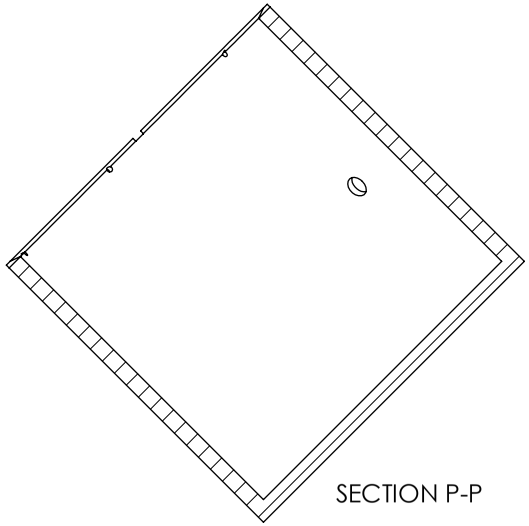

SECTION P-P

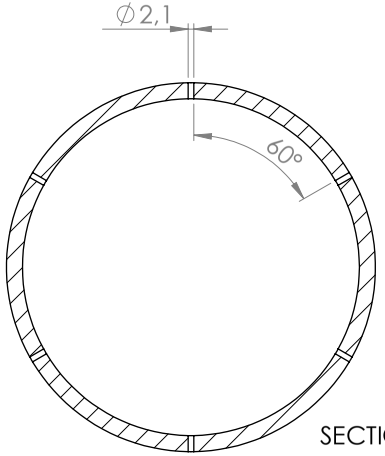

SECTION K-K

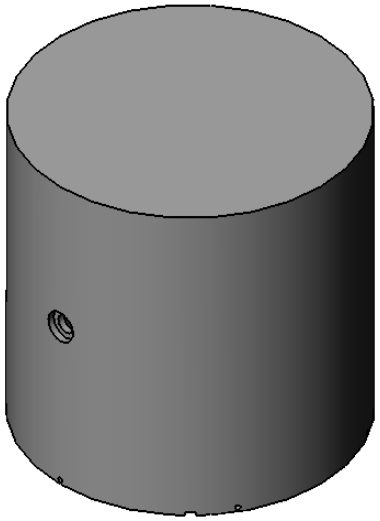

UNLESS OTHERWISE SPECIFIED: DIMENSIONS ARE IN MILLIMETERS SURFACE FINISH: TOLERANCES: LINEAR: ANGULAR:		FINISH:		DEBUR AND BREAK SHARP EDGES		DO NOT SCALE DRAWING	REVISION
	NAME	SIGNATURE	DATE			TITLE:	
DRAWN							
CHK'D							
APPV'D							
MFG							
Q.A				MATERIAL:		DWG NO. Heat shield outer	A3
				WEIGHT:		SCALE:1:2	SHEET 1 OF 1

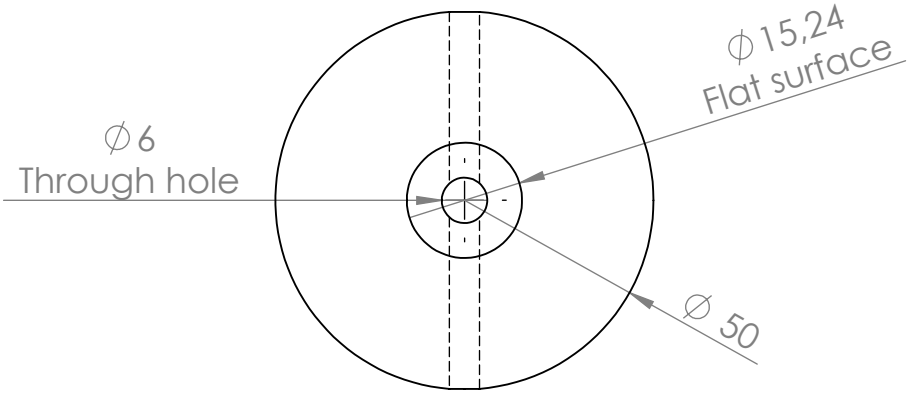

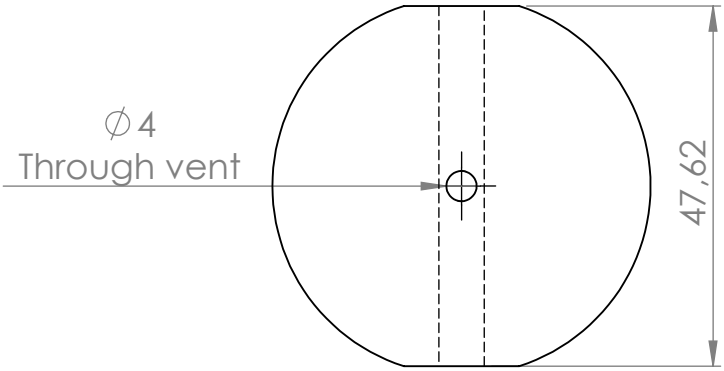

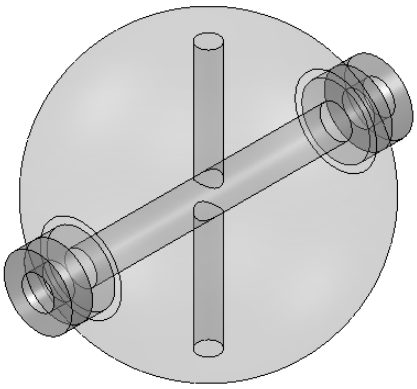

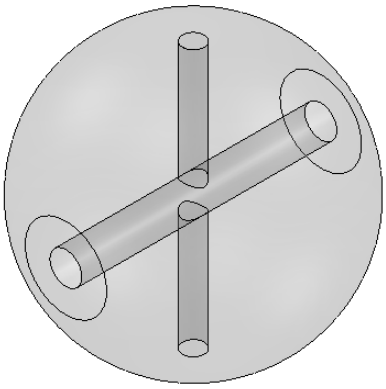

Complete cavity, spacer with mirrors and compensation rings mounted.

UNLESS OTHERWISE SPECIFIED: DIMENSIONS ARE IN MILLIMETERS SURFACE FINISH: TOLERANCES: LINEAR: ANGULAR:	FINISH:		DEBUR AND BREAK SHARP EDGES		DO NOT SCALE DRAWING	REVISION
	NAME	SIGNATURE	DATE			TITLE:
DRAWN						
CHK'D						
APPV'D						
MFG						
Q.A				MATERIAL:	DWG NO.	A4
					ULE cavity spacer	
				WEIGHT:	SCALE:1:1	SHEET 1 OF 1

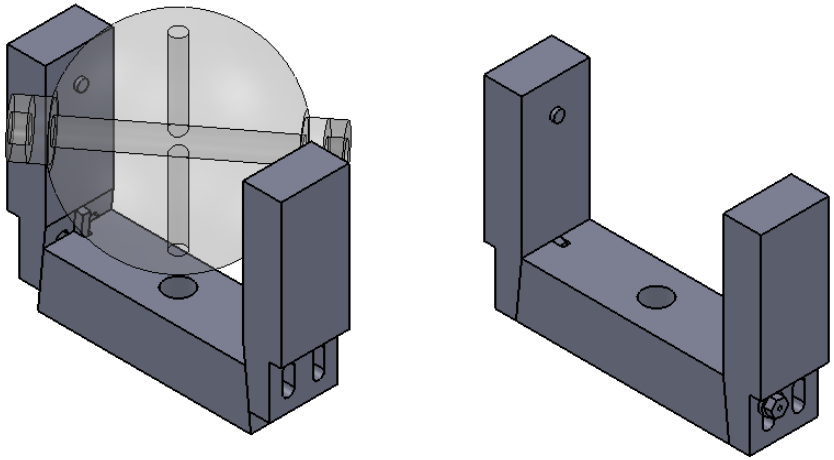

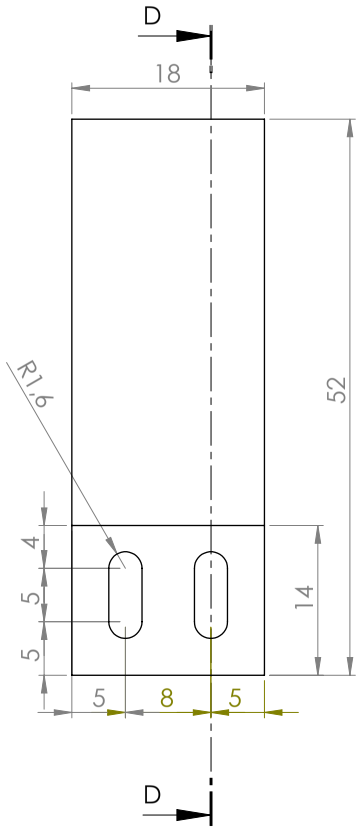

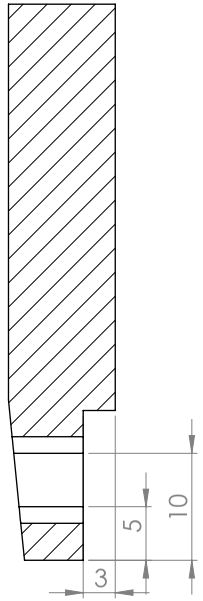

SECTION D-D
SCALE 2 : 1

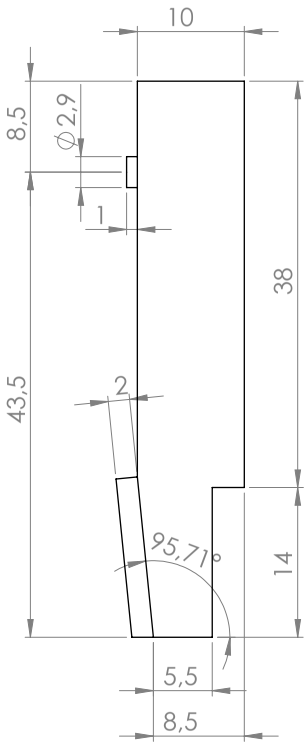

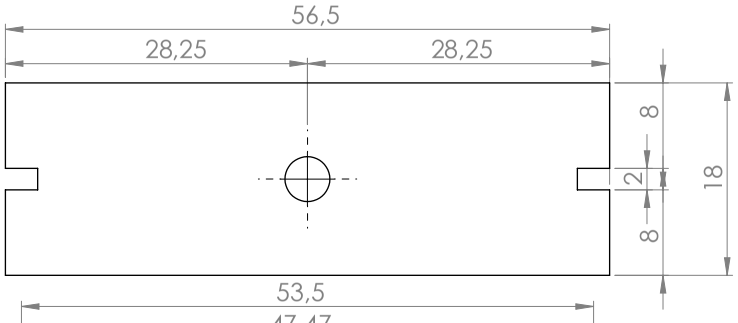

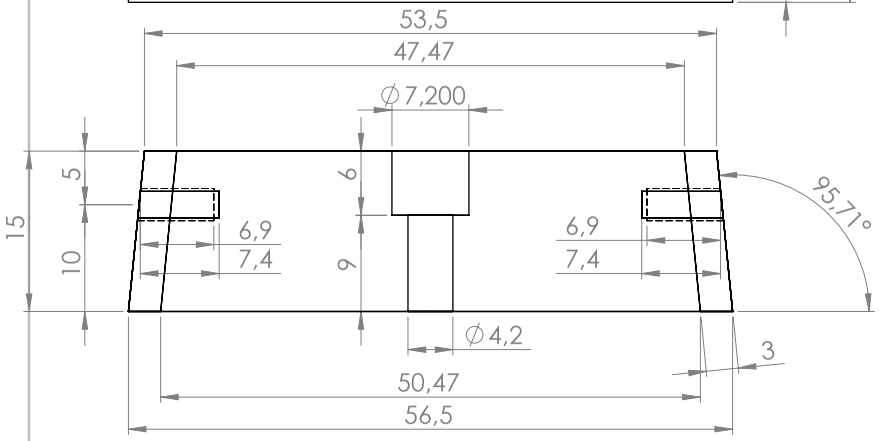

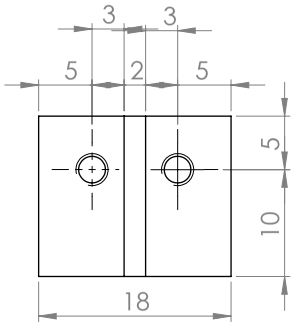

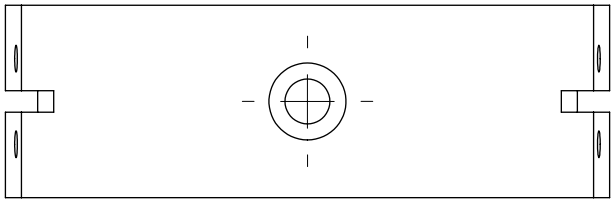

UNLESS OTHERWISE SPECIFIED: DIMENSIONS ARE IN MILLIMETERS SURFACE FINISH: TOLERANCES: LINEAR: ANGULAR:		FINISH:		DEBUR AND BREAK SHARP EDGES		DO NOT SCALE DRAWING	REVISION
	NAME	SIGNATURE	DATE			TITLE:	
DRAWN							
CHK'D							
APPV'D							
MFG							
Q.A				MATERIAL:		DWG NO. Cavity holder	A3
				WEIGHT:		SCALE:1:1	SHEET 1 OF 1

Diese Zeichnung ist Eigentum der VACOM Vakuum Komponenten & Messtechnik GmbH.
Sie darf nur mit ausdrücklicher Genehmigung kopiert, verwertet oder an Dritte weitergegeben werden.

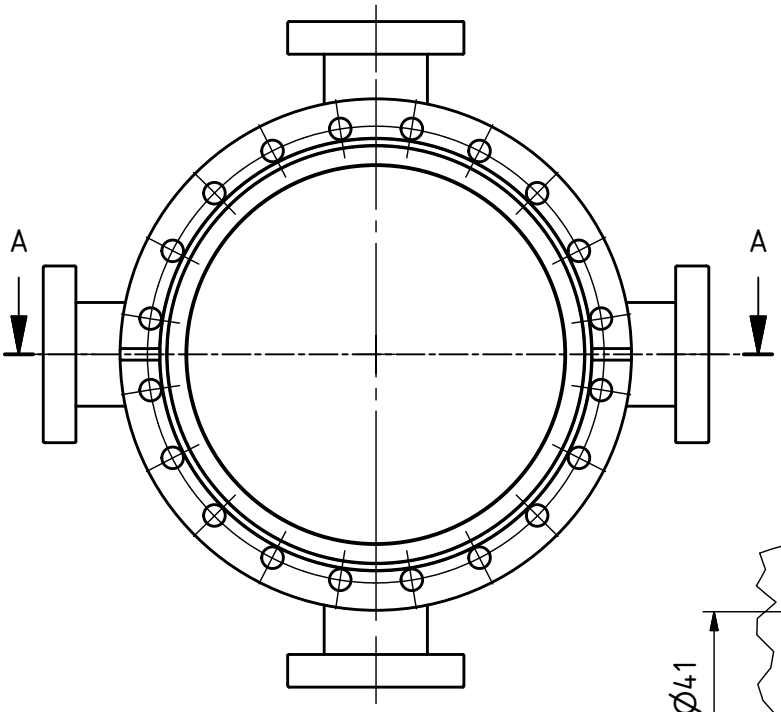

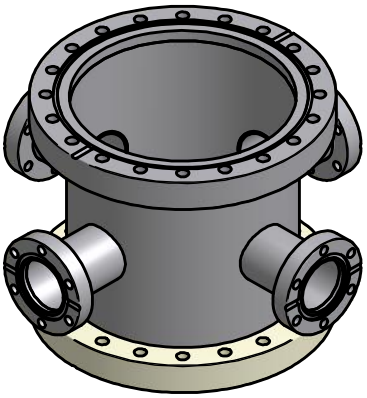

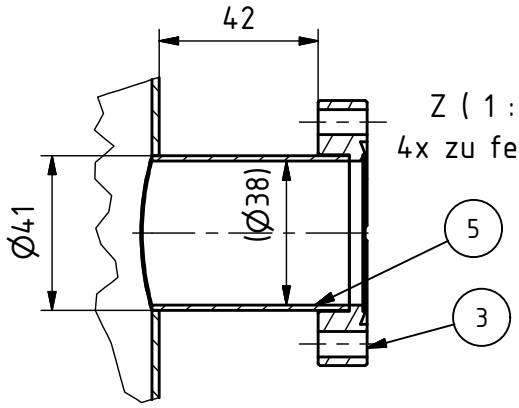

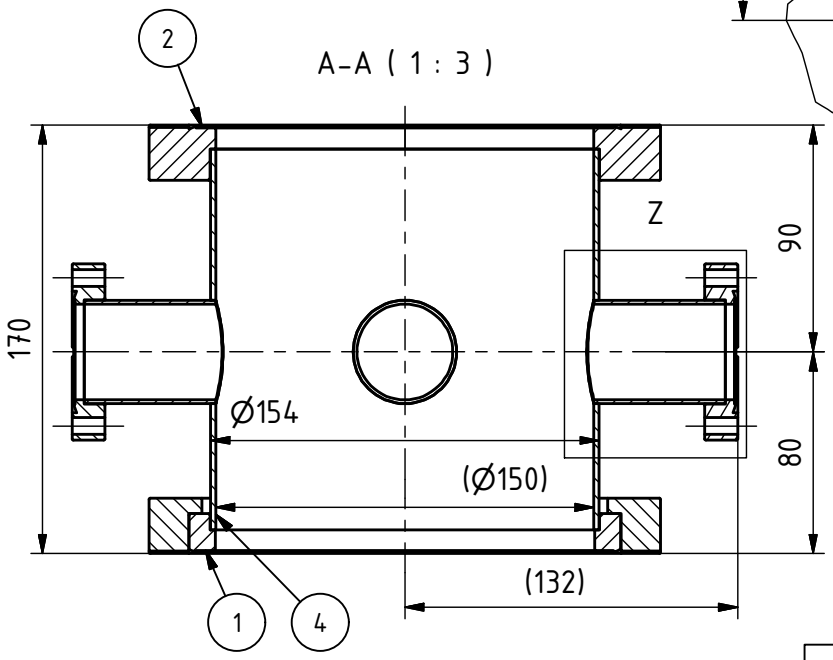

ATTENTION!
Ports not centered 170 to measure

Welded on vacuum side
Plane and smooth weld seams
Tubes mechanically polished on the vacuum side
bead blasted on atmospherical side
Protect sealing faces
Test for leaks < 10^{-9} mbar l/s

Stückliste

Pos.	Anzahl	Mat.Nr.	Mat.-Kurztext
1	1	300647	F160RB154-304
2	1	300622	F160B154-304
3	4	300813	F40B41-304
4		100605	R14404-154X2.0-11866
5		100606	R14404-41X1.5-11866

Toleranz										
spanend: Toleranz	ISO 2768-m	0.5...3	± 0.1	>3...6	± 0.1	>6...30	± 0.2	>30...120	± 0.3	>120...400	± 0.5	>400...1000	± 0.8
Schweißtoleranz	ISO 13920 B	2...30	± 1	>30...400	± 2								
Schweißtoleranz	ISO 13920 F	30...120	± 1.0	>120...400	± 1.5	>400...1000	± 3.0						

VACOM Vakuum Komponenten & Messtechnik GmbH

Änderung d. Kunden	Freigabe durch Kunden
Name, Datum	Name, Datum

Oberflächen nach DIN EN ISO 1302: Ra 3,2 (Ra 0.8)

Kanten nach DIN ISO 13715: -0,2 / +0,4

Maßstab:	1:3 (1:2 1:5)	Werkstoff:	304/316L	6,736 kg

Vorgänger:
Ersatz:

Freigabe durch Vacom
Name, Datum

erstellt von:	Heidi Nittner
erstellt am:	18.04.2011
geprüft von:	
geprüft am:	
Toleranzen:	ISO2768 mK ISO13920 BF

SPE-10018550-20

Vacuum chamber CF160 with 4 lateral ports CF40, height 170mm

312102 | Oberfläche in mm² 383086,6 mm^2 | Blatt 1 / 1

J:\drawings inventor\special\CF\SPE-10018550-20\SPE-10018550-20_KND.idw | A4

Zust.	Änderungen	Datum	Name

Diese Zeichnung ist Eigentum der VACOM Vakuum Komponenten & Messtechnik GmbH.
Sie darf nur mit ausdrücklicher Genehmigung kopiert, verwertet oder an Dritte weitergegeben werden.

spanend: Toleranz	0.5...3	>3...6	>6..30	>30..120	>120..400	>400..1000
	±0.1	±0.1	±0.2	±0.3	±0.5	±0.8
ISO 2768-m						

Schweißtoleranz	2..30	>30..400	30..120	>120..400	>400..1000
ISO 13920 B	±1	±2	±1.0	±1.5	±3.0
ISO 13920 F					

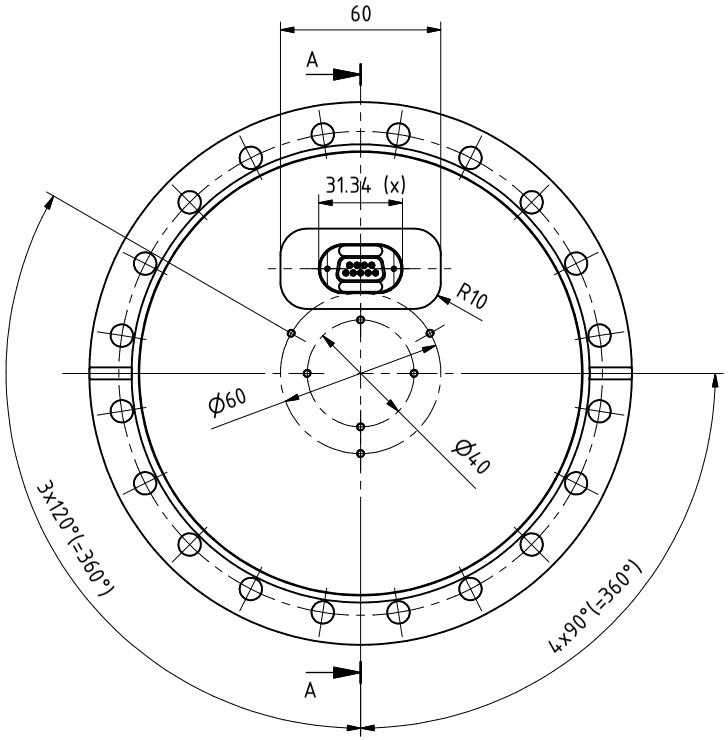

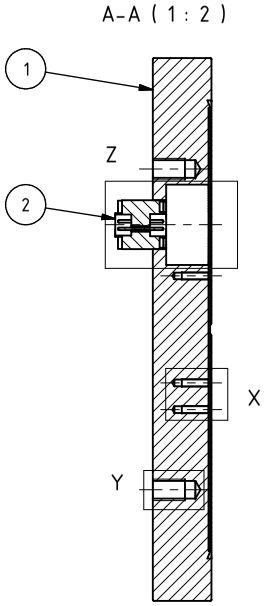

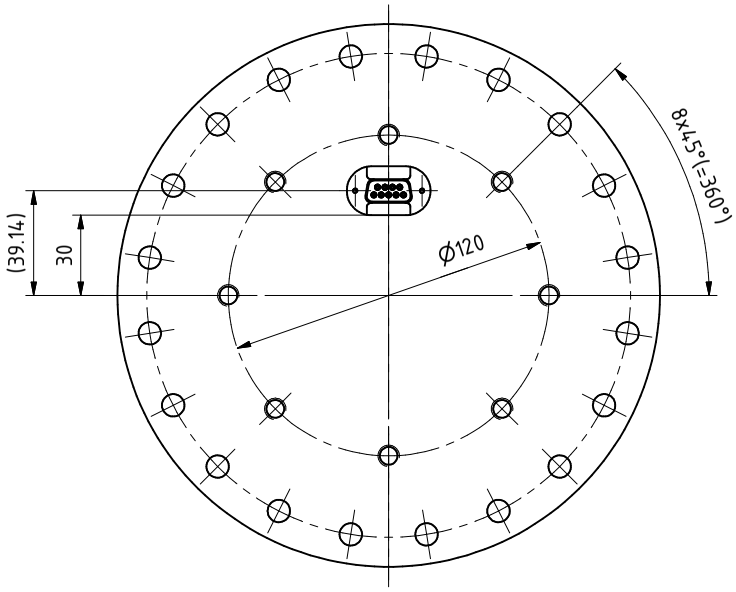

(x) Ø der Bohrungen an
Durchführung anpassen

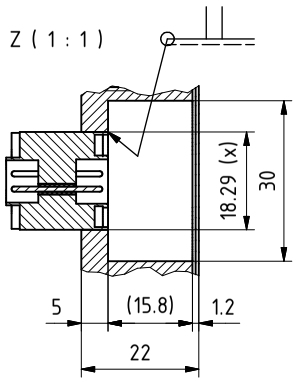

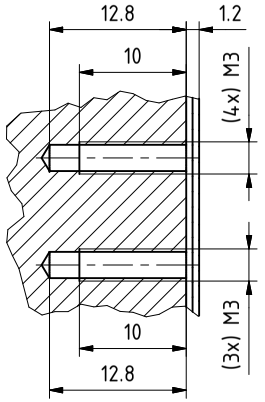

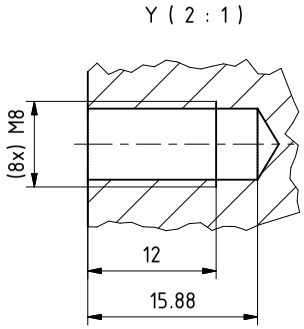

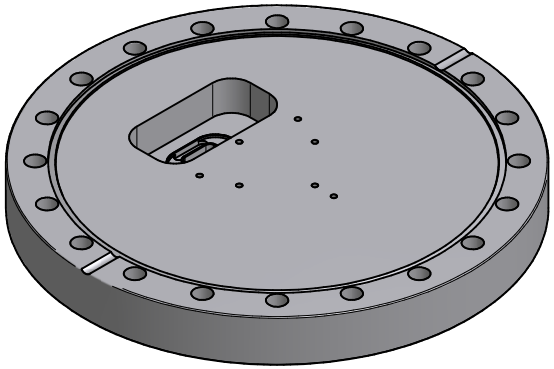

1x Durchführung W-SUBD-9-DE-CE-SSG
Schweißlippe 31.34±0.05 x 18.29±0.05
Leitermaterial Edelstahl vergoldet
Leiterdurchmesser 9x1.0mm

vakuumseitig schweißen
flache und glatte Schweißnähte
Anlauffarben entfernt
lecktesten < 10^{-9}mbar l/s

Stückliste			
Pos.	Anzahl	Mat.Nr.	Mat.-Kurztext
1	1	300611	F160-304
2	1	101002	W-SUBD-9-DE-CE-SSG

10^{-n} mbar VACOM
VACOM Vakuum Komponenten & Messtechnik GmbH

Änderung d. Kunden	Freigabe durch Kunden	Oberflächen nach DIN EN ISO 1302	Kanten nach DIN ISO 13715
Name, Datum	Name, Datum	Ra 3,2 (Ra 0,8)	-0,2 +0,4

Vorgänger:		Freigabe durch Vacom	Maßstab: 1:2 (2:1 1:1)	Werkstoff: 304 / 1.4301	5.076 kg
Ersatz:		Name, Datum	erstellt von: Sven Haser	SPE-10018890-10	
			erstellt am: 18.04.2011	Vacuum special flange CF DN160	
			geprüft von:	acording to customers drawing	
			geprüft am:		
Zust.	Änderungen	Datum / Name	Toleranzen: ISO2768 mK / ISO13920 BF	312226	Oberfläche in mm² 99350,2 mm^2	Blatt 1 / 1
				J:\drawings inventor\special\CF\SPE-10018890-10\SPE-10018890-10.idw	A3

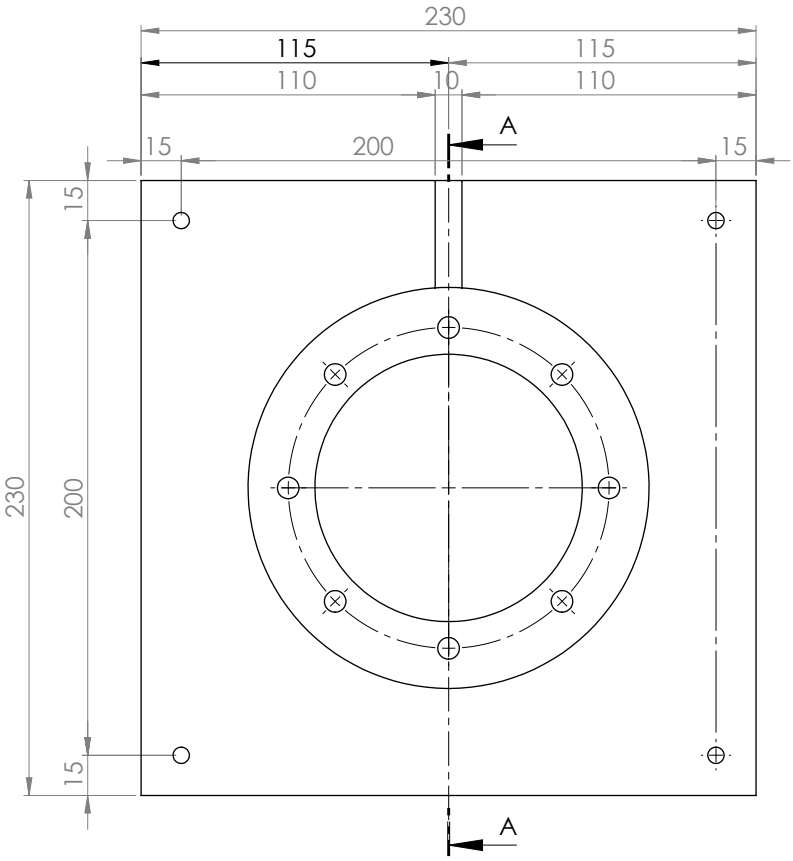

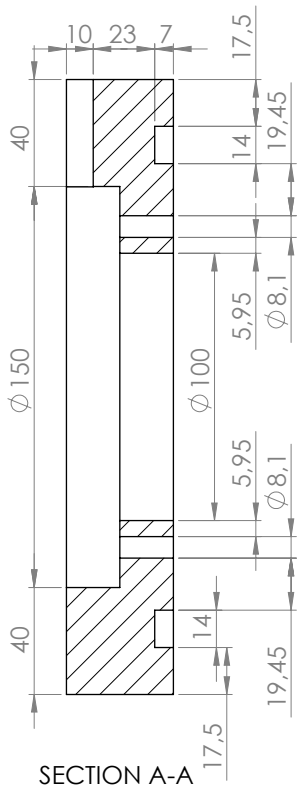

SECTION A-A
SCALE 1 : 2

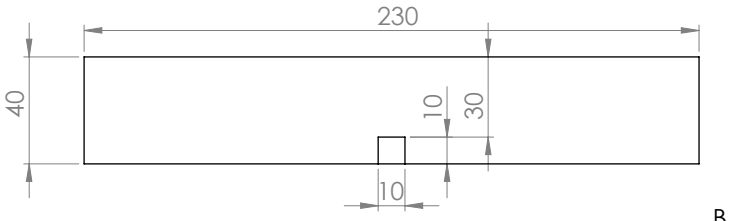

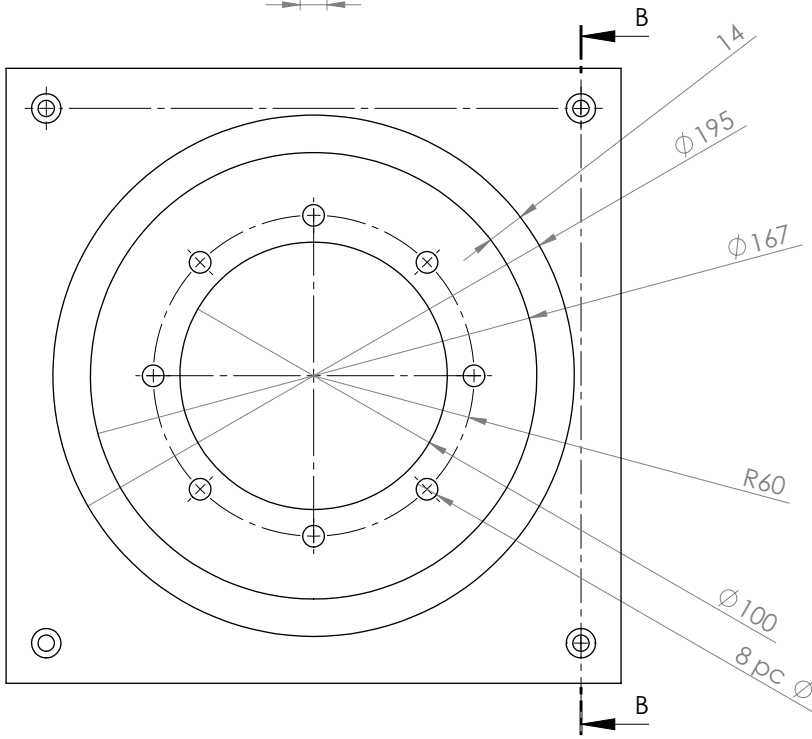

SECTION B-B
SCALE 1 : 2

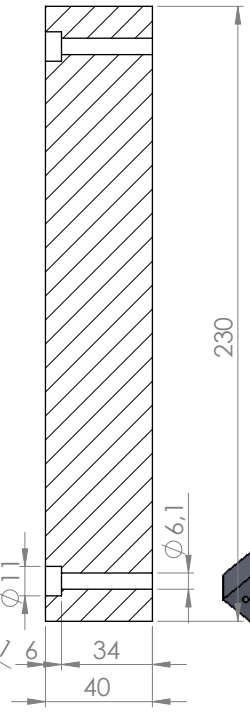

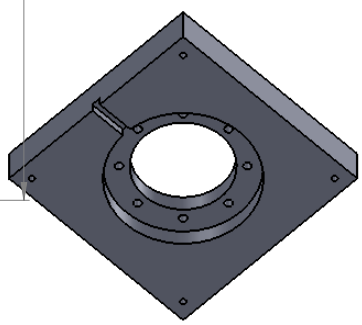

Vaccum chamber mount

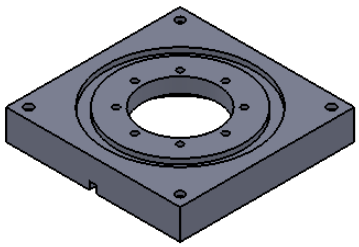

B

Circuit diagrams

B7700
DC voltage to current converter.

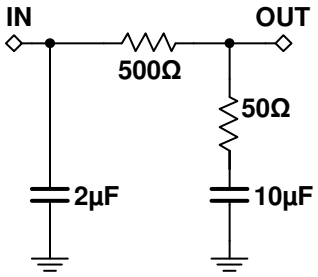

B5900
Low frequency amplifier

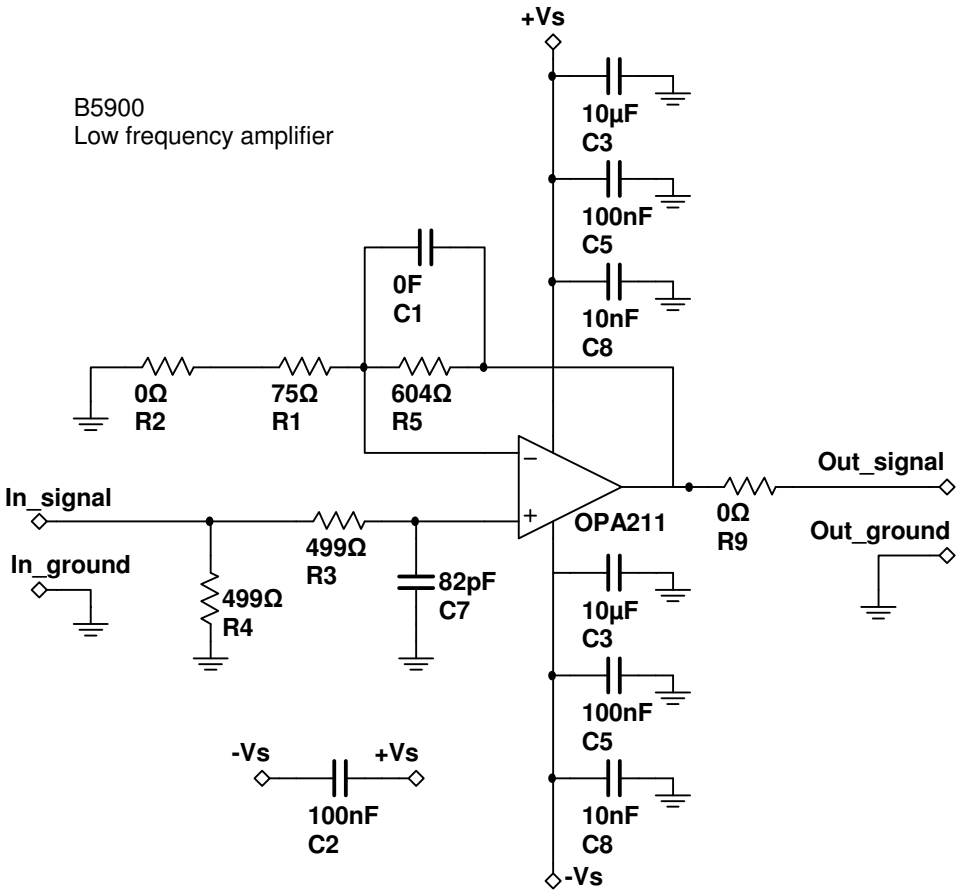

C Code

```
% Function that calculates the matrix multiplications the correct way.
function [out] = mult(M,V)
out = [ (M(1,1)*V(1)+M(1,2))/(M(2,1)*V(1)+M(2,2))  ; 1 ];


% Function that calculates the spotsize and vergence from the q-parameter.
function out = calc_par(q,lambda)
q=1/q;
R = 1/real(q);
w = sqrt(-lambda/(pi*imag(q)));
out = [R, w];
```

```
% Program using ABCD transfer matrices to calculate the spotsize and
% vergence of the laser beam.

clear all
i = sqrt(-1);

n_BK7 = 1.515;      % Refractive index of BK7 at 610 nm.
n_FS = 1.459;       % Refractive index of fused silica at 590 nm.
n_0 = 1;

lambda = 593e-9;    % Light wavelength, m

r_CavMir = 0.5;     % Radius of curvature, cavity mirror, m
d_cav = 48.7e-3;    % Distance between mirror inside cavity, m

% Matrix describing the system studied, formatted according to the
% following format; [ type pos n surface_value ].
%
% - "type" means, Flat surface = 1, Curved surface = 2, Lens = 3.
% - "pos" is the distance from the first point on the
%   optical axis of the system studied to the lens/surface.
% - "n" is the refractive index of the medium after the lens/surface.
% - The "surface_value" is a parameter describing the lens/surface. For a
%   lens it's the focal length and for a surface it's the radius of curvature.

sys_mat  = [ 1  0          n_0     0          % End flat cavity mirror
             2  48.7e-3     n_FS    -0.5       % Start curved cavity mirror
             1  55.05e-3    n_0     0          % End curved cavity mirror
             1  72.54e-3    n_BK7   0          % Start isolating glass 1
             1  75.54e-3    n_0     0          % End isolating glass 1
             1  84.54e-3    n_BK7   0          % Start isolating glass 2
             1  87.54e-3    n_0     0          % End isolating glass 2
             1  156.28e-3   n_BK7   0          % Start vacuum window
             1  166.28e-3   n_0     0          % End vacuum window
             3  450e-3      n_0     430e-3 ];  % Coupling lens

sys_mat = sortrows(sys_mat,2);

% Initial beam properties given by the size and shape of the cavity
```

```
% Using formulas given in Lasers, p751 (by Siegman)
% to calculate spotsize inside cavity.
g = 1 - d_cav/r_CavMir;
w_1 = sqrt(d_cav*lambda/pi*sqrt(g/(1-g)))      % Spotsize at plane mirror
q_i = (-i*lambda/(pi*w_1^2))^(-1);             % Initial complex beam parameter

dl = 0.1e-3;    % Steplength, m
d = 0:dl:1;    % Beam length studied, m

% Initialize varibles needed in the iteration loop
data = zeros(length(d),2);
i = 0;
q_plot = q_i;
q = q_i;
n = n_0;
n_prev = n_0;

for pos=d
   i = i+1;
   no_surface = 1;

   for comp_pos = sys_mat(:,2)'
      % Controll if pos is in the vecinty of any surface
      if(pos >= comp_pos && pos < comp_pos+dl)
         no_surface = 0;

         % Get the data about the surface at current pos
         [r,c] = find(sys_mat(:,2) == comp_pos);
         comp_vec = sys_mat(r,:);

         % Update the value of the refractive index
         n_prev = n;
         n = comp_vec(3);

         % Check which type of component and calc transfer matrix
         switch comp_vec(1)
            % Flat surface
            case 1
               T = [ 1 0 ; 0 n_prev/n ];
               % Curved surface
```

```
            case 2
                T = [ 1 0 ; (n_prev-n)/(comp_vec(4)*n) n_prev/n ];
                % Thin lens
            case 3
                T = [ 1 0 ; -1/comp_vec(4) 1 ];
                lins = 1
        end

        % Calculat new q value and update q_plot and pos
        q = mult(T,[q;1]);
        q_plot = q;

        % If the current component isn't the last one calculate effect
        % of free space propagation to the next component.
        [r_max c_max] = size(sys_mat);
        if( r_max > r)
            next_comp_pos = sys_mat(r+1,2);
            L = next_comp_pos - comp_vec(2);
            T = [ 1 L ; 0 1 ];
            q = mult(T,[q;1]);
        end
    end
end

% In case pos is not close to any surface, just calculates a small
% step in free space.
if(no_surface)
    T = [ 1 dl ; 0 1 ];
    q_plot = mult(T,[q_plot;1]);
end

% Save spotsize and vergenc for each small step
data(i,:) = calc_par(q_plot(1),lambda/n);
end

% Plot vergence
figure(1)
hold on
plot(d*1000,data(:,1)*1000,'r');
title('Vergence');
```